



HAL
open science

Helium isotope variations between Réunion Island and the Central Indian Ridge (17°–21°S): New evidence for ridge–hot spot interaction

Evelyn Füre, David R. Hilton, Bramley J. Murton, Christophe C Hémond, Jérôme Dymont, James M. Day

► **To cite this version:**

Evelyn Füre, David R. Hilton, Bramley J. Murton, Christophe C Hémond, Jérôme Dymont, et al.. Helium isotope variations between Réunion Island and the Central Indian Ridge (17°–21°S): New evidence for ridge–hot spot interaction. *Journal of Geophysical Research: Solid Earth*, 2011, 116 (B2), pp.B02207. 10.1029/2010JB007609 . insu-01309301

HAL Id: insu-01309301

<https://insu.hal.science/insu-01309301>

Submitted on 29 Apr 2016

HAL is a multi-disciplinary open access archive for the deposit and dissemination of scientific research documents, whether they are published or not. The documents may come from teaching and research institutions in France or abroad, or from public or private research centers.

L'archive ouverte pluridisciplinaire **HAL**, est destinée au dépôt et à la diffusion de documents scientifiques de niveau recherche, publiés ou non, émanant des établissements d'enseignement et de recherche français ou étrangers, des laboratoires publics ou privés.

Helium isotope variations between Réunion Island and the Central Indian Ridge (17°–21°S): New evidence for ridge–hot spot interaction

Evelyn Fürti,^{1,2} David R. Hilton,¹ Bramley J. Murton,³ Christophe Hémond,⁴ Jérôme Dymont,⁵ and James M. D. Day⁶

Received 29 March 2010; revised 22 November 2010; accepted 10 December 2010; published 24 February 2011.

[1] We report new helium abundance and isotope results for submarine basaltic glasses from the Central Indian Ridge (CIR) between the Marie Celeste (16.7°S) and Egeria fracture zones (FZ) (20.6°S); the adjacent Gasitao, Three Magi, and Rodrigues ridges; and for olivine separates from lavas and cumulate xenoliths from the Mascarene Islands (Réunion, Mauritius, and Rodrigues). Helium isotope ratios in basaltic glasses range from 7.1 to 12.2 R_A (where $R_A = \text{air } ^3\text{He}/^4\text{He}$) and lie between values of Mid-Ocean Ridge Basalt (MORB) ($8 \pm 1 R_A$) and samples from Réunion Island (11.5 to 14.1 R_A). The highest $^3\text{He}/^4\text{He}$ values (up to 12.2 R_A) are found in glasses recovered off axis from the Three Magi and Gasitao ridges. Along the CIR axis, MORB-like $^3\text{He}/^4\text{He}$ ratios are found near the Egeria FZ, and there is a marked increase to values of $\sim 11 R_A$ between $\sim 19^\circ$ and 20°S . The lowest $^3\text{He}/^4\text{He}$ values ($< 8 R_A$) are found immediately south of the Marie Celeste FZ, where incompatible trace element ratios (e.g., La/Sm) are highest. These low $^3\text{He}/^4\text{He}$ ratios can be explained by closed system radiogenic ^4He ingrowth in either (1) a “fossil” Réunion hot spot mantle component, embedded into the subridge mantle when the CIR migrated over the hot spot at ~ 34 Ma or (2) trace element enriched MORB mantle. In contrast, the high $^3\text{He}/^4\text{He}$ ratios observed on the CIR axis adjacent to the Gasitao Ridge, and along the off-axis volcanic ridges, are consistent with flow of hot spot mantle material from Réunion (~ 1100 km to the west) toward the CIR.

Citation: Fürti, E., D. R. Hilton, B. J. Murton, C. Hémond, J. Dymont, and J. M. D. Day (2011), Helium isotope variations between Réunion Island and the Central Indian Ridge (17°–21°S): New evidence for ridge–hot spot interaction, *J. Geophys. Res.*, 116, B02207, doi:10.1029/2010JB007609.

1. Introduction

[2] Geophysical and geochemical observations have revealed that a significant portion of the global mid-ocean ridge system is influenced by hot spots, located within ~ 1400 km of the ridge axis [Schilling, 1991]. In locations where a hot spot is close to a spreading ridge (e.g., Iceland, Amsterdam–St. Paul, Azores, Easter, Galápagos, and Réunion), lateral flow of upwelling hot spot mantle along the base of

the lithosphere toward and along the ridge system results in increased melt production and crustal thickness, as well as elevated topography and negative gravity anomalies at the ridge axis [Ito and Lin, 1995a, 1995b; Dymont et al., 2007]. Furthermore, mixing of hot spot mantle with the subridge mantle generates enriched trace element signatures (e.g., high La/Sm ratios) as well as variations in Sr, Nd, and Pb isotope ratios of basalts erupted at the ridge [Hart et al., 1973; Schilling, 1973; Schilling et al., 1982; Schilling et al., 1985; Hanan et al., 1986; Ito et al., 2003].

[3] Mid-ocean ridge basalts (MORB) sampled away from the influence of hot spots display $^3\text{He}/^4\text{He}$ ratios of $8 \pm 1 R_A$ (where $R_A = ^3\text{He}/^4\text{He}$ of air), whereas hot spot–derived ocean islands basalts (OIB) from Iceland, Hawaii, Galápagos, Samoa and Réunion show higher $^3\text{He}/^4\text{He}$ ratios [see Graham, 2002, and references therein]. Nearly all of Earth’s ^3He is primordial (i.e., it was trapped during Earth formation), whereas ^4He is continuously produced by the radioactive decay of U and Th. Thus, the distinct helium signatures of MORB and OIB suggest that the MORB source has evolved with a higher time-integrated (U+Th)/ ^3He ratio than the source(s) of hot spot magmas. Consequently, helium isotopes are a powerful tool for studying ridge–hot spot

¹Fluids and Volatiles Laboratory, Geosciences Research Division, Scripps Institution of Oceanography, University of California, San Diego, La Jolla, California, USA.

²Now at Centre de Recherche Pétrographiques et Géochimiques, Nancy Université, Vandœuvre-lès-Nancy, France.

³National Oceanography Centre, University of Southampton, Southampton, UK.

⁴UMR “Domaines océaniques,” Institut Universitaire Européen de la Mer, Plouzané, France.

⁵Laboratoire Géosciences Marines, CNRS UMR 7154, Institut de Physique du Globe de Paris, Paris, France.

⁶Department of Geology, University of Maryland, College Park, Maryland, USA.

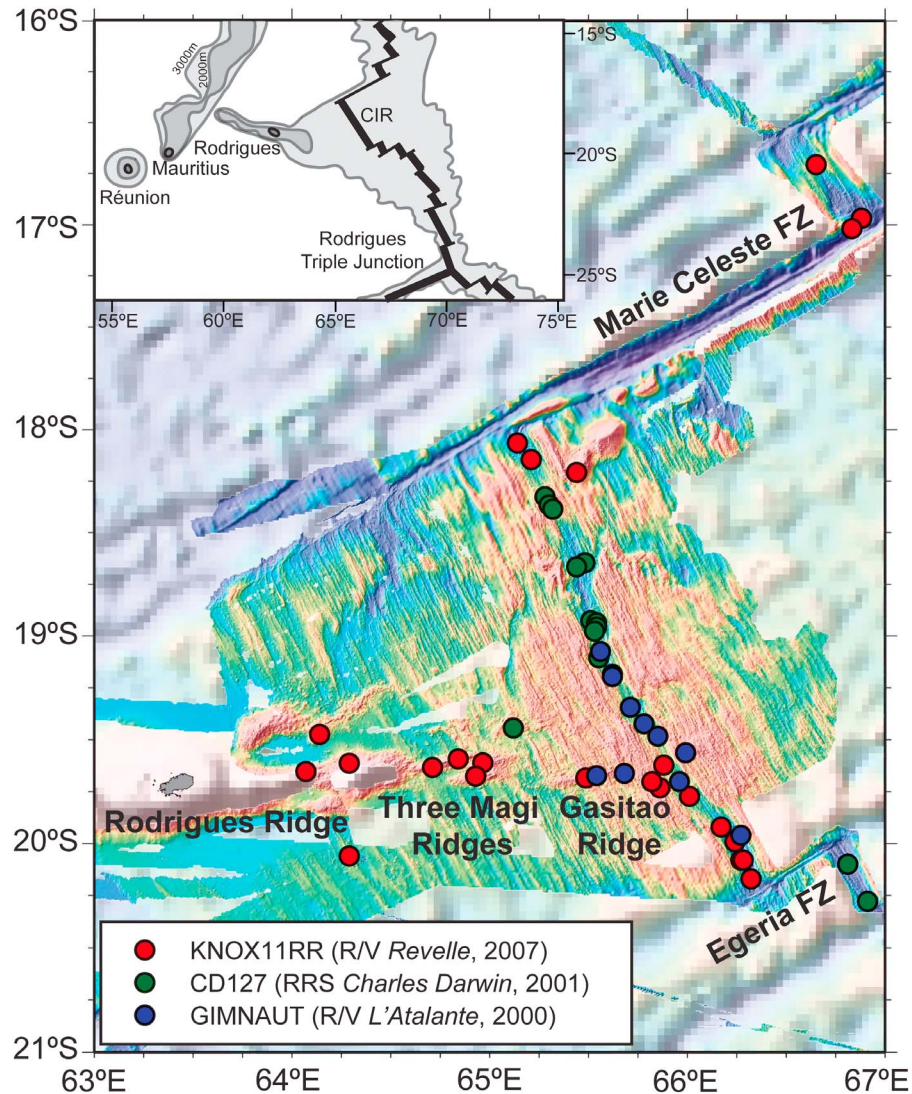


Figure 1. Bathymetric map of the CIR and the adjacent Gasitao Ridge, the Three Magi Ridges, and the Rodrigues Ridge. The three levels of color for the bathymetry data represent (1) pale colors, bathymetry “predicted” from satellite altimetry [Smith and Sandwell, 1997]; (2) intermediate colors, previous multibeam bathymetric data from R/V *Marion Dufresne* (1998 [Dyment et al., 1999]), *L’Atalante* (2000 [Dyment et al., 2000]), and *Hakuho-Maru* (2007 [Okino et al., 2008]); (3) bright colors, multibeam bathymetric data collected by R/V *Revelle* (2007 [Füri et al., 2008]). The circles indicate the location of samples collected during the KNOX11RR (red), CD127 (green), and GIMNAUT (blue) cruises. The inset shows the Mascarene Islands (Réunion, Mauritius, and Rodrigues) to the west of the CIR as well as the Rodrigues Triple Junction.

interaction: introduction of high $^3\text{He}/^4\text{He}$ mantle material from a nearby hot spot to the subridge mantle should generate MORB lavas with high helium isotope ratios. Within the Indian Ocean Basin, for example, marked increases in $^3\text{He}/^4\text{He}$ ratios, up to $14.1 R_A$ and $16.4 R_A$, have been observed on the Southwest Indian Ridge near the Bouvet hot spot [Kurz et al., 1998] and on the Southeast Indian Ridge near the Amsterdam-St. Paul hot spot [Graham et al., 1999; Burnard et al., 2002; Nicolaysen et al., 2007], respectively.

[4] In this contribution, we explore the interaction between the Central Indian Ridge (CIR) and the off-axis Réunion hot spot. We performed an extensive helium isotope and abundance survey along the CIR axis between

16.7°S and 20.6°S, and the adjacent Gasitao Ridge, Three Magi Ridges, and Rodrigues Ridge (Figure 1). In addition, we determined the helium isotope and abundance characteristics of olivine separates from a suite of lavas and cumulate xenoliths from the Mascarene Islands (Réunion, Mauritius, and Rodrigues). The new data set shows that some basaltic glasses from the CIR and off-axis volcanic ridges record a Réunion-like helium isotope signature. These observations permit us to evaluate the dynamics of mixing between different mantle components in this region of the Indian Ocean Basin, together with the effects of shallow level magmatic processes (i.e., post-eruptive radiogenic ^4He ingrowth, degassing and fractional crystallization)

that also play a role in establishing the helium characteristics of the erupted lavas.

2. Geologic Setting and Background

[5] The CIR, which separates the African and Indo-Australian plates, extends southward from the Carlsberg Ridge near the equator toward the Rodrigues Triple Junction (20.5°S, 70°E), where it branches into the Southeast and the Southwest Indian ridges. In this study, we target the CIR segment bounded by the Marie Celeste FZ (Fracture Zone) to the north and the Egeria FZ to the south (Figure 1). The CIR axis is shallowest along this segment, and offsets shift it westward toward the island of Réunion [Parson *et al.*, 1993].

[6] At ~34 Ma, the northeastward migrating CIR passed over the Réunion hot spot [Duncan *et al.*, 1990], which is presently located ~1100 km to the west of the ridge axis. The Réunion hot spot formed the Deccan Trap flood basalts, the Chagos-Maldives-Laccadive Ridge, the Mascarene Plateau, as well as the Mascarene Islands, composed of the islands of Réunion, Mauritius, and Rodrigues [Duncan *et al.*, 1989, 1990]. Réunion Island represents the most recent expression of the hot spot. The island is composed of two volcanoes: Piton des Neiges, which was active between ~2 Ma and 43 ka, and the still active Piton de la Fournaise, where volcanic activity began ~530 ka ago [Gillot and Nativel, 1989]. Mauritius is considered to be located on the former site of the Réunion hot spot [Morgan, 1981; Paul *et al.*, 2005]. Volcanic activity on Mauritius started with a shield-building stage at 8 to 7 Ma (Older Series), with later stages at 3 to 2 Ma (Intermediate Series) and 0.7 to 0.2 Ma (Younger Series) [McDougall and Chamalaun, 1969]. Rodrigues Island was formed at 1.5 Ma [McDougall *et al.*, 1965]; it lies at the eastern end of the Rodrigues Ridge, an east-west trending volcanic ridge that is 8 to 10 Ma old [Duncan *et al.*, 1990]. Smaller en-échelon volcanic ridges at 19°S (the Three Magi Ridges and the Gasitao Ridge) appear to extend the Rodrigues Ridge to the near vicinity of the CIR (Figure 1) [Dyment *et al.*, 1999, 2000].

[7] A number of models have been proposed to explain the occurrence of volcanism between the Mascarene Islands and the CIR. Morgan [1978] proposed that the Rodrigues Ridge was formed by volcanism above a channel of upwelling Réunion hot spot mantle, deflected toward the ridge axis as the CIR migrated northeastward away from the hot spot. In this scenario, a geochemical signature from the Réunion hot spot would be expected on the CIR axis at ~19.5°S, i.e., at the intersection of the ridge axis with a line projected through Réunion and Rodrigues islands. While Mahoney *et al.* [1989] found a Réunion-like isotope signature (low $^{143}\text{Nd}/^{144}\text{Nd}$, high $^{87}\text{Sr}/^{86}\text{Sr}$, high $^{207}\text{Pb}/^{204}\text{Pb}$, and high $^{206}\text{Pb}/^{204}\text{Pb}$) in basalt glasses from the CIR, the geochemical anomaly was only observed in the vicinity of the Marie Celeste FZ, i.e., further north than predicted by Morgan [1978]. A more detailed study showed that basalts collected between the Marie Celeste FZ and the Rodrigues Triple Junction record a systematic decrease in incompatible element concentrations and ratios (e.g., La/Sm) toward the south [Murton *et al.*, 2005]. These trace element and radiogenic isotope characteristics of CIR basalts have been interpreted to reflect the presence of an enriched mantle

source near the Marie Celeste FZ and normal MORB-like mantle in the south. Given these constraints, Mahoney *et al.* [1989] and Murton *et al.* [2005] proposed that Réunion hot spot mantle is migrating eastward along the Marie Celeste FZ toward the CIR, where it is forced southward and mixes with depleted MORB mantle.

[8] To investigate in more detail the influence of the Réunion hot spot on the CIR, Nauret *et al.* [2006] targeted a suite of basalts collected both on and off the CIR axis between 18° and 20°S. While they confirmed that basalts from the North generally have higher incompatible trace element ratios than southern samples, they concluded that the composition of Réunion lavas (derived from three submarine samples collected from the flanks of Piton de la Fournaise; [Fretzdorff and Haase, 2002]) is not suitable as an end-member for the observed Sr-Nd-Pb isotope characteristics of most on-axis samples. Only off-axis lavas from the Gasitao Ridge, as well as a single on-ridge sample collected at 19.95°S, appeared to record a Réunion source signature. Therefore, Nauret *et al.* [2006] proposed that Réunion hot spot material flows eastward toward the CIR on a trajectory that impinges the ridge at ~19.9°S, which agrees with the scenario initially described by Morgan [1978], and they concluded that the mantle source enrichment in the vicinity of the Marie Celeste FZ, ~100 km to the north, cannot be related to influx of mantle material from Réunion. However, we note that more recently published trace element and Sr-Nd-Pb isotope data demonstrate that the Réunion hot spot is more heterogeneous than previously thought [e.g., Luais, 2004; Vlastélic *et al.*, 2005; Bosch *et al.*, 2008; Pietruszka *et al.*, 2009]. Consequently, the source of Réunion lavas can represent a suitable mixing end-member for the isotope signature of CIR basalts sampled between 18° and 20°S.

[9] While trace element and Sr-Nd-Pb isotope data clearly show the presence of an enriched component in the subridge mantle of the CIR, the only helium isotope ratios that have been reported so far from this region of the CIR were for four basaltic glasses and range from 7.26 to 8.96 R_A [Mahoney *et al.*, 1989], virtually undistinguishable from the range associated with depleted MORB mantle ($8 \pm 1 R_A$ [Graham, 2002]). In contrast, both historic and prehistoric lavas from Piton de la Fournaise, the presently active volcano on La Réunion, show that the Réunion hot spot is characterized by significantly higher $^3\text{He}/^4\text{He}$ ratios of ~11.8 to 14.5 R_A [Kaneoka *et al.*, 1986; Staudacher *et al.*, 1986; Graham *et al.*, 1990; Staudacher *et al.*, 1990; Hanyu *et al.*, 2001; Trieloff *et al.*, 2002; Hopp and Trieloff, 2005]. Thus, any interaction of the CIR with the Réunion hot spot is expected to result in helium isotope values greater than $8 \pm 1 R_A$ in basalts erupted along the ridge axis.

3. Sampling and Analytical Techniques

[10] We collected submarine pillow basalts by dredging during the KNOX11RR cruise (November 2007) of the R/V *Revelle* along the CIR axis (between 16.7°S and 20.1°S), and the adjacent Gasitao Ridge, Three Magi Ridges, and Rodrigues Ridge [Füri *et al.*, 2008]. We recovered variable amounts of fresh glass from 24 out of a total of 38 dredge locations (Figure 1). This sample set was supplemented by 12 glass samples from the GIMNAUT cruise [Nauret *et al.*,

2006] and 14 glass samples from the cruise CD127 [Murton *et al.*, 2005]. In addition, subaerial olivine phenocryst-rich lavas on Rodrigues, Mauritius, and Réunion, as well as cumulate xenoliths from Piton Chisny (Réunion), were collected during field sampling in November 2007. The xenoliths range from fresh dunites to highly oxidized dunites with red discoloration.

[11] Submarine glasses from the GIMNAUT cruise [Nauret *et al.*, 2006] and from cruise CD127 [Murton *et al.*, 2005] were analyzed for major elements by electron microprobe, and trace element abundances were determined using an ICP-MS PlasmaQuad turbo 2+ and laser ablation ICP-MS, respectively. The KNOX11RR major element data were obtained from whole rock samples by wavelength dispersive XRF spectrometry, and picked glasses were analyzed for trace elements using a Thermo X-series II ICP-MS. Reference standards BHVO-2 and BIR-1 were run during the XRF data acquisition, with additional standards JB1A and JB-3 for the ICP-MS analyses, and yield accuracy and precision values for the KNOX11RR data (auxiliary material Tables S1 and S2).¹ Major and/or trace element data could not be obtained for some dredge locations with small sample yields.

[12] Olivine separates from lavas and xenoliths from the Mascarene Islands were analyzed by electron microprobe at Washington State University. For each sample, between 6 and 12 grains of olivine were analyzed for their major element chemistry in order to calculate their Mg numbers ($=\text{Mg}/(\text{Mg} + \text{Fe}^{2+}) \times 100$).

[13] A total of 51 basaltic glass samples, as well as 21 olivine separates, were analyzed for their helium isotope and abundance characteristics on a MAP 215 noble gas mass spectrometer by crushing. In the case of glasses, we selected fresh chips, free of phenocrysts and surface alteration using a binocular microscope. For phenocrysts, we ensured that crystals had no adhering matrix. In all cases, an effort was made to choose a small number of large grains to minimize the surface area to volume ratio and help preserve vesicles and/or inclusions in the samples. However, olivine phenocrysts from Rodrigues and Mauritius are significantly smaller than the phenocrysts in lavas from Réunion.

[14] After precleaning in a 1:1 acetone-methanol mixture, approximately 50 to 170 mg of glass (i.e., typically between 1 to 10 chips) or 0.5 to 1 g of olivines, respectively, were loaded into online, electromagnetic crushers (see description by Scarsi [2000]) connected to the preparation line of the MAP 215 noble gas mass spectrometer and pumped overnight to ultrahigh vacuum. Crushing of the samples was achieved by externally accelerating a magnetized steel slug up and down within the crusher for 2 min at a frequency of ~120 impacts per minute. For basaltic glass, most He (>60%) will reside in the vesicle phase even at low degrees of vesicularity (~1%) [e.g., Jambon *et al.*, 1986; Carroll and Draper, 1994]. Since crushing physically pulverizes the glass and releases vesicle-sited volatiles, it is expected that helium abundances obtained by crushing will closely approximate the total “magmatic” helium content of the submarine glasses utilized in this study (within a factor of ~2). In the case of olivine separates, in contrast, He is extracted

from inclusions adopting the technique of short crushing times (2 min). Short crushing times minimize release of matrix-sited He [Hilton *et al.*, 1993] where implanted radiogenic He is likely to reside. Although we cannot rule out liberation of some matrix-sited He if present, it is unlikely that it contributes significantly to the inclusion He released by crushing. Therefore, we consider measured olivine $^3\text{He}/^4\text{He}$ ratios in young (Réunion) samples as representing unmodified magmatic values; however, in the case of older samples (i.e., from Mauritius and Rodrigues), we regard these as minimum values (see section 4.1).

[15] The volatiles released upon crushing were purified in the mass spectrometer preparation line by sequential exposure to a 750°C hot Ti getter, an activated charcoal trap (held at -196°C), a SAES getter, and a cryogenic trap lined with activated charcoal (held at <20 K). Helium was released from the cryogenic trap by increasing the temperature to 35 K, whereas Ne was released at 90 K. Sample $^3\text{He}/^4\text{He}$ ratios and $^4\text{He}/^{20}\text{Ne}$ ratios were measured in static mode and calibrated against standard aliquots of air (=1 R_A) run at least twice a day under identical experimental conditions. Prior to each individual sample run, an analytical blank of the entire system was measured. The blanks (average $\leq 0.5 \times 10^{-9}$ cm³STP⁴He) were subtracted from each sample helium measurement. The blank contribution to the ^4He signal was less than 0.5% for all basaltic glass samples (except for the exceptionally He-poor sample D29-1) and xenoliths from Piton Chisny. In contrast, olivine phenocrysts from lavas showed a significantly higher blank contribution between 1 and 11% for samples from Réunion, and between 7 and 65% for samples from Mauritius and Rodrigues due to low He contents and/or small sample sizes. Furthermore, analytical blanks for ^{20}Ne were subtracted from each sample neon measurement, with any remaining neon considered an estimate of air-derived ^{20}Ne in the sample. However, only samples D29-1, RU07-11, and RG07-01 showed a significant air ^{20}Ne contribution, as indicated by low X values of 3.5, 22.3, and 4.5, respectively, where $X = (^4\text{He}/^{20}\text{Ne})_{\text{sample}} / (^4\text{He}/^{20}\text{Ne})_{\text{air}}$. Therefore, we corrected the measured helium isotope ratios and helium concentrations of these three samples for the effects of air contamination (see Tables 1 and 2 for details).

4. Results

[16] Helium isotope ratios ($^3\text{He}/^4\text{He}$) and concentrations for olivine separates from the Mascarene Islands are reported in Table 1. Helium isotope compositions and abundances, as well as chondrite-normalized La/Sm ratios, for 51 submarine basalt glasses from the central Indian Ocean are given in Table 2. In addition, major and trace element concentrations for glasses collected during the KNOX11RR cruise are reported in Tables S1 and S2, respectively. Helium isotope ratios are reported in the form of R/R_A, where R is the $^3\text{He}/^4\text{He}$ ratio measured in the sample and R_A is the atmospheric $^3\text{He}/^4\text{He}$ ratio of 1.4×10^{-6} . For samples RG07-01, RU07-11, and D29-1, indicated in bold in Tables 1 and 2, we report air-corrected helium isotope ratios (R_c/R_A) and abundances ([He]_c) due to small but significant air contributions recorded in these samples.

¹Auxiliary materials are available in the HTML. doi:10.1029/2010JB007609.

Table 1. Helium Characteristics of Olivine Separates From Mascarene Islands Lavas and Xenoliths^a

Sample ID ^b	Latitude ^c (S)	Longitude ^c (E)	Age/Unit ^d	Weight (mg)	³ He/ ⁴ He (R/R _A)	[He] cm ³ STP/g (×10 ⁻⁹)	Mg Number ^e
<i>Rodrigues</i>							
RG07-01	19°40'53.5"	63°24'57.7"		425.2	5.35 ± 0.43	1.45 ± 0.01	80.9 ± 2.0 (n = 10)
RG07-14	19°41'55.2"	63°27'10.4"		688.9	5.60 ± 0.67	0.53 ± 0.01	83.4 ± 2.2 (n = 12)
RG07-15	19°40'07.1"	63°27'24.0"		488.8	7.43 ± 0.41	0.98 ± 0.01	81.1 ± 2.1 (n = 10)
RG07-17	19°44'55.1"	63°23'24.7"		615.8	8.40 ± 0.25	5.28 ± 0.01	79.0 ± 2.5 (n = 12)
RG07-20	19°41'45.4"	63°23'33.1"		542.1	8.41 ± 0.21	11.81 ± 0.02	82.8 ± 3.3 (n = 10)
<i>Mauritius</i>							
MR07-05	20°26'54.5"	57°20'48.8"	Older Series	541.6	8.64 ± 0.77	0.72 ± 0.01	83.3 ± 2.2 (n = 10)
MR07-06	20°13'00.0"	57°29'56.0"	Older Series	497.3	7.71 ± 0.37	1.85 ± 0.01	84.5 ± 0.4 (n = 10)
MR07-09	20°20'09.8"	57°46'44.3"	Older Series	650.3	10.36 ± 0.29	5.71 ± 0.01	82.7 ± 0.8 (n = 8)
MR07-10	20°21'16.5"	57°44'40.4"	Older Series	483.1	7.36 ± 0.33	1.97 ± 0.01	83.7 ± 1.3 (n = 9)
<i>La Réunion</i>							
RU07-01B	21°13'08.2"	55°48'25.4"	PDLF 4 (AD2002)	1068.4	12.53 ± 0.22	18.32 ± 0.02	84.2 ± 0.2 (n = 10)
RU07-02	21°13'15.1"	55°48'26.2"	PDLF 4 (AD1931)	1080.9	12.88 ± 0.31	14.09 ± 0.01	84.0 ± 0.2 (n = 10)
RU07-03	21°13'20.0"	55°48'23.3"	PDLF 4 (AD1998)	479.5	12.45 ± 0.52	15.20 ± 0.03	84.0 ± 0.7 (n = 6)
RU07-05	21°16'45.4"	55°47'43.1"	PDLF 4 (AD2007)	736.2	13.71 ± 0.20	10.43 ± 0.01	84.5 ± 0.2 (n = 10)
RU07-08	21°15'18.2"	55°42'08.3"	PDLF 4 (AD1937)	959.8	12.61 ± 0.27	20.31 ± 0.02	83.3 ± 0.6 (n = 10)
RU07-10	21°53'14.6"	55°26'24.9"	Younger Oceanite Series	904.3	12.54 ± 0.28	3.05 ± 0.01	87.7 ± 0.9 (n = 10)
RU07-11	21°53'11.0"	55°26'15.2"	Younger Oceanite Series	701.1	11.96 ± 0.54	2.39 ± 0.01	88.0 ± 0.5 (n = 10)
RU07-12	21°55'52.4"	55°23'29.4"	Younger Oceanite Series	1019.7	12.84 ± 0.23	14.40 ± 0.01	84.3 ± 0.4 (n = 11)
CH07-01	21°13'53.6"	55°39'44.3"	PDLF 3	831.7	13.95 ± 0.25	917.27 ± 0.21	85.3 ± 0.5 (n = 11)
CH07-02	21°13'49.9"	55°39'55.8"	PDLF 3	669.7	13.66 ± 0.22	195.23 ± 0.11	85.3 ± 0.1 (n = 10)
CH07-04	21°13'49.8"	55°39'57.1"	PDLF 3	834.7	14.09 ± 0.23	157.99 ± 0.05	84.5 ± 0.3 (n = 11)
CH07-07	21°13'52.1"	55°39'55.9"	PDLF 3	893.3	13.58 ± 0.15	367.20 ± 0.09	84.1 ± 0.3 (n = 10)

^aAll errors are reported at the 1σ level.

^bSamples labeled CH07-0X represent dunite xenoliths collected at Piton Chisny, Piton de la Fournaise (Réunion). For the two samples in bold, we report air-corrected He isotope ratios and He contents, i.e., $R_C/R_A = [(R/R_A \times X) - 1]/(X - 1)$ and $[He]_C = ([He] \times (X - 1))/X$, where $X = ({}^4\text{He}/{}^{20}\text{Ne})/({}^4\text{He}/{}^{20}\text{Ne})_{\text{air}}$. Measured He isotope ratios are 4.1 R_A for sample RG07-01 and 11.5 R_A for sample RU07-11. No air correction was needed for all other samples.

^cLatitude and Longitude determined by GPS measurement (WGS 84 datum). In degrees, minutes and seconds.

^d"Older Series," shield-building stage (7–8 Ma) of Mauritius [McDougall and Chamalaun, 1969]; "Younger Oceanite Series," Piton des Neiges (0.43–2.1 Ma); PDLF3: Piton de la Fournaise, Phase 3 (5–60 ka); "PDLF4," Piton de la Fournaise, Phase 4 (present–5 ka) [Chevallier and Bachelery, 1981; Chevallier and Vatin-Perignon, 1982; Montaggioni and Nativel, 1988].

^eMg number = $[\text{Mg}/(\text{Mg} + \text{Fe}^{2+})] \times 100$; n = number of olivine grains analyzed.

4.1. Olivine Separates From the Mascarene Islands (Réunion, Mauritius, Rodrigues)

[17] The helium contents of four olivine separates from dunite xenoliths collected at Piton Chisny (Réunion; CH07-0X) range from 158 to 917 (×10⁻⁹ cm³STP/g) (Table 1 and Figure 2a). In contrast, the helium abundances of all olivine phenocrysts from the Mascarene Islands lavas are significantly lower and vary between 0.5 and 20.3 (×10⁻⁹ cm³STP/g). Phenocrysts from Mauritius and Rodrigues, i.e., the smallest olivine grains, show the lowest helium abundances. Mg numbers of the olivine separates range from 79.0 ± 2.5 to 88.0 ± 0.5 (Table 1 and Figure 2b). We note that olivine grains within individual samples from Mauritius and Rodrigues show a wider range in Mg numbers than those from samples collected on Réunion. This may reflect larger variations of the Mg/Fe ratio within the sampled melt fractions, as well as possible reequilibration of the smaller-sized Mauritius and Rodrigues olivines with their host melt. This interpretation is consistent with generation of olivine from variably degassed, fractionated and contaminated melts, as observed in other volcanic settings [e.g., Hilton et al., 1993, 1995; Day et al., 2005]. The range in Mg numbers (and ³He/⁴He ratios) observed in olivines from Réunion is limited, consistent with homogenization of magma compositions by magma chamber processing beneath Piton de la Fournaise

[e.g., Graham et al., 1990; Pietruszka et al., 2009, and references therein].

[18] The new helium isotope ratios for olivine phenocrysts and xenoliths from Réunion vary between 11.9 and 14.1 R_A and agree with the values observed in previous studies (~11.8 to 14.5 R_A [Kaneoka et al., 1986; Staudacher et al., 1986; Graham et al., 1990; Staudacher et al., 1990; Hanyu et al., 2001; Trieloff et al., 2002; Hopp and Trieloff, 2005]). The mean ³He/⁴He ratios of phenocrysts from Piton des Neiges (Younger Oceanite Series) and Piton de la Fournaise (PDLF 4) are 12.45 ± 0.45 R_A (n = 5) and 12.84 ± 0.51 R_A (n = 3), respectively, whereas xenoliths from Piton Chisny (PDLF 3) show slightly higher values of 13.82 ± 0.24 R_A (n = 4). The difference between the R/R_A values of xenoliths and erupted lavas may reflect more extensive degassing of the host lavas compared to the cumulate xenoliths, followed by ingrowth of ⁴He* and/or crustal contamination of olivines within lava samples.

[19] The ³He/⁴He ratios of olivine phenocrysts from Mauritius and Rodrigues are significantly lower and range from 7.4 to 10.4 R_A and 5.3 to 8.4 R_A, respectively. These results compare well with the data set of Hanyu et al. [2001], where ³He/⁴He ratios of ~11.8 R_A for Older Series lavas on Mauritius, and a value of ~8 R_A for two samples from Rodrigues were reported; however, these authors were unable to determine the He isotope composition of

Table 2. Helium Systematics of Submarine Basaltic Glasses From the CIR Axis and the Adjacent Gasitao, Three Magi, and Rodrigues Ridges^a

Sample ID	Latitude ^b (°S)	Longitude ^b (°E)	Depth (m)	Weight (mg)	³ He/ ⁴ He (R/R _A)	[He] cm ³ STP/g (×10 ⁻⁹)	(La/Sm) _N ^c
<i>CIR Axis</i>							
D1-1 ^d	-16.70	66.65	3146	75.0	8.11 ± 0.11	12264 ± 13	1.12
D3-3 ^d	-16.96	66.88	4272	82.6	7.91 ± 0.02	12719 ± 3	1.36
D3-9 ^d	-16.96	66.88	4272	79.8	7.96 ± 0.02	11423 ± 4	1.34
D2-1 ^d	-17.01	66.83	4038	77.3	8.19 ± 0.09	17022 ± 4	1.13
D8-2 ^d	-18.05	65.14	3202	75.3	7.08 ± 0.14	4532 ± 7	1.22
D9-1 ^d	-18.13	65.21	3127	71.2	7.25 ± 0.08	11710 ± 2	1.58
RC19 ^e	-18.31	65.28	2823	124.6	7.61 ± 0.05	2333 ± 1	1.47
RC20 ^e	-18.35	65.3	2788	134.6	7.46 ± 0.04	5305 ± 2	1.72
RC21 ^e	-18.37	65.32	2765	124.9	7.51 ± 0.04	6671 ± 2	1.82
RC7 ^e	-18.63	65.48	2996	69.4	8.38 ± 0.03	5642 ± 1	1.31
RC5 ^e	-18.65	65.44	3120	57.9	9.38 ± 0.04	2785 ± 1	1.25
RC10 ^e	-18.91	65.51	3064	135.6	10.86 ± 0.06	5434 ± 2	0.81
RC12 ^e	-18.92	65.54	3099	132.5	9.80 ± 0.07	15010 ± 4	0.79
RC13 ^e	-18.94	65.54	3039	65.2	7.24 ± 0.03	17675 ± 5	0.73
RC4 ^e	-18.96	65.53	3068	54.5	8.96 ± 0.06	8987 ± 2	1.34
DR11-1 ^f	-19.05	65.56	3020	73.0	9.19 ± 0.16	705 ± 1	1.31
RC1 ^e	-19.09	65.55	2853	51.6	9.72 ± 0.11	805 ± 1	2.09
PL20-2 ^f	-19.17	65.62	2695	110.2	9.02 ± 0.03	9776 ± 3	0.53
PL01-5 ^f	-19.18	65.62	3012	106.7	9.50 ± 0.03	10897 ± 3	0.89
DR06-1 ^f	-19.33	65.71	2885	59.4	9.81 ± 0.15	5088 ± 2	0.97
DR05-1 ^f	-19.41	65.78	3061	67.6	8.86 ± 0.10	1353 ± 1	0.64
PL11-1 ^f	-19.47	65.85	2879	52.1	8.97 ± 0.09	2295 ± 1	0.54
DR02-3 ^f	-19.55	65.99	2120	56.9	8.65 ± 0.07	7854 ± 2	0.59
DR01-1 ^f	-19.55	65.94	2130	54.3	10.57 ± 0.03	3598 ± 1	0.80
D17-1 ^d	-19.61	65.88	2742	112.8	8.76 ± 0.02	1867 ± 1	0.97
DR03-1 ^f	-19.69	65.96	2990	60.6	8.83 ± 0.07	6464 ± 2	0.82
D15-1 ^d	-19.76	66.01	2794	76.6	8.68 ± 0.01	7401 ± 4	0.62
D14-1 ^d	-19.91	66.17	3267	73.4	8.46 ± 0.02	5987 ± 1	0.72
DR10-1 ^f	-19.95	66.27	3070	114.5	10.31 ± 0.06	573 ± 1	0.59
D13-1 ^d	-19.98	66.24	3511	67.4	8.26 ± 0.03	3004 ± 3	0.51
D12-2 ^d	-20.07	66.27	3550	71.3	8.41 ± 0.03	4275 ± 1	0.54
D11-2 ^d	-20.07	66.28	3370	71.1	8.46 ± 0.03	1540 ± 1	n.d.
D10-2 ^d	-20.16	66.32	3483	71.1	8.38 ± 0.04	1537 ± 1	0.49
D6 ^e	-20.09	66.81	3900	61.8	8.24 ± 0.07	2941 ± 1	0.69
RC23 ^e	-20.27	66.91	3520	63.8	8.11 ± 0.04	1866 ± 1	0.41
RC18 ^e	-20.6	68.2	2853	54.2	9.03 ± 0.09	688 ± 1	0.54
<i>Seamount</i>							
D6-2 ^d	-18.22	65.41	2048	72.6	7.18 ± 0.03	1270 ± 3	1.19
<i>Gasitao Ridge</i>							
D18-2 ^d	-19.72	65.86	2216	119.8	9.09 ± 0.06	470 ± 1	0.95
D19-2 ^d	-19.69	65.82	2176	118.2	8.72 ± 0.05	2453 ± 1	0.51
DR09-1 ^f	-19.65	65.68	2071	61.1	10.58 ± 0.19	8496 ± 2	0.59
DR08-1 ^f	-19.66	65.54	2110	59.6	12.10 ± 0.18	4954 ± 2	0.45
				48.5	12.21 ± 0.17	2727 ± 127	
D20-5 ^d	-19.70	65.49	2002	114.8	8.28 ± 0.05	3949 ± 8	0.49
<i>Three Magi Ridges</i>							
D5_1.5 ^e	-19.43	65.12	2226	54.0	10.24 ± 0.11	4197 ± 1	1.74
D22-1 ^d	-19.62	64.97	1687	128.9	9.28 ± 0.06	7128 ± 12	n.d.
				61.0	9.52 ± 0.01	11425 ± 3	
D24-6 ^d	-19.67	64.95	2019	158.3	10.32 ± 0.09	430 ± 1	0.42
D25-2 ^d	-19.58	64.84	2123	156.4	9.48 ± 0.04	358 ± 1	0.71
D26-2 ^d	-19.62	64.71	1785	119.5	9.51 ± 0.02	5103 ± 4	0.75
<i>Rodrigues Ridge</i>							
D29-1^d	-19.60	64.29	1820	124.3	8.97 ± 1.21	2.2 ± 0.1	1.65
D34-1 ^d	-19.46	64.14	2134	119.0	8.72 ± 0.03	650 ± 1	0.64
D30-3 ^d	-19.64	64.07	2156	135.0	9.95 ± 0.17	10551 ± 9	0.59
<i>Abyssal Hill</i>							
D37-2 ^d	-20.05	64.29	2833	171.3	9.67 ± 0.17	219 ± 1	0.91

^aAll errors are reported at the 1 σ level. For sample D29-1, indicated in bold, we report the air-corrected He isotope ratio and He content, i.e., R_C/R_A = [(R/R_A × X) - 1]/(X - 1) and [He]_C = ([He] × (X - 1))/X, where X = (⁴He/²⁰Ne)/(⁴He/²⁰Ne)_{air}. The measured He isotope ratio is 7.2 R_A. All other samples required no air correction. n.d. No data available.

^bLatitude and Longitude (i.e., dredge on bottom coordinates) from R/V *Revelle* shipboard computer.

^c(La/Sm)_N is the chondrite-normalized La/Sm ratio, i.e., (La/Sm)_N = (La/Sm)_m/(La/Sm)_{Cl}, where (La/Sm)_{Cl} ≈ 1.6 [McDonough and Sun, 1995].

^dSamples collected on the KNOX11RR cruise (R/V *Revelle*, 2007 [Füri et al., 2008]).

^eSamples collected on the CD127 cruise (RRS *Charles Darwin*, 2001 [Murton et al., 2005]).

^fSamples collected on the GIMNAUT cruise (R/V *L'Atalante*, 2000 [Nauret et al., 2006]).

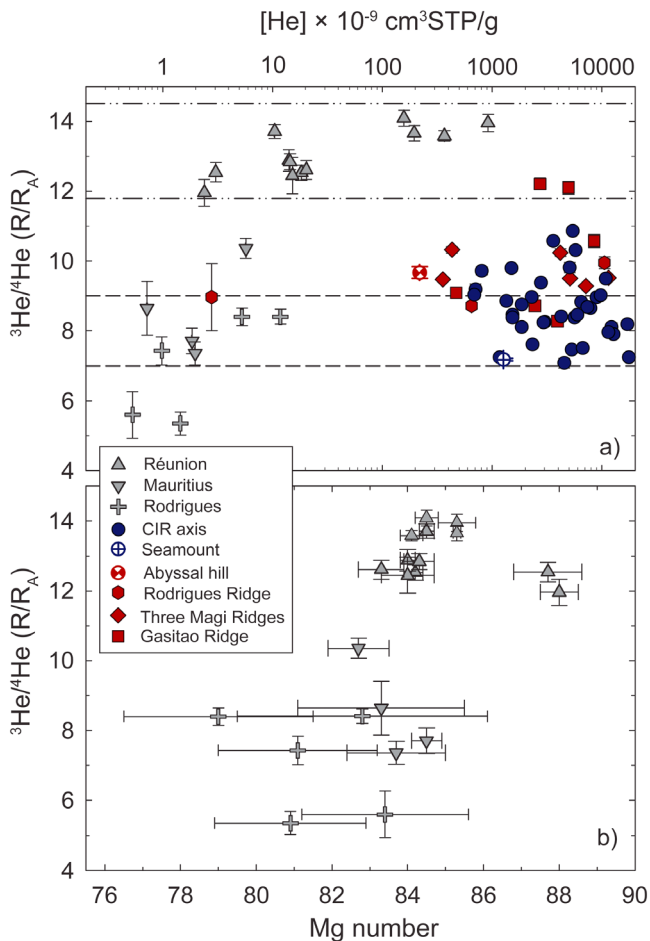


Figure 2. (a) Helium isotope ratios ($^3\text{He}/^4\text{He}$) versus helium concentrations of olivine separates from lavas and xenoliths from the Mascarene Islands (Réunion, Mauritius, and Rodrigues) as well as of submarine basaltic glasses from the CIR axis, the Rodrigues Ridge, the Three Magi Ridges, and the Gasitao Ridge. The horizontal dashed lines indicate the range of values expected for MORB ($8 \pm 1R_A$ [Graham, 2002]) and the composition of lavas from Réunion Island ($\sim 11.8\text{--}14.5 R_A$ [Kaneoka et al., 1986; Staudacher et al., 1986; Graham et al., 1990; Staudacher et al., 1990; Hanyu et al., 2001; Trieloff et al., 2002; Hopp and Trieloff, 2005]). (b) $^3\text{He}/^4\text{He}$ ratios of olivines are plotted as a function of their measured Mg numbers. Olivine phenocrysts in lavas from Mauritius and Rodrigues record a wider range in Mg numbers compared to olivines sampled in Réunion Island lavas (see section 4.1).

8 out of 17 samples due to low helium abundances ($<0.3 \times 10^{-9} \text{ cm}^3 \text{ STP/g}$).

[20] Figure 2a shows that olivine separates with low He abundances tend to have low $^3\text{He}/^4\text{He}$ ratios. The lowest $^3\text{He}/^4\text{He}$ values are measured in samples from Mauritius and Rodrigues (i.e., the phenocrysts with the lowest He contents) whereas the highest $^3\text{He}/^4\text{He}$ ratios are preserved in xenoliths from Piton Chisny. In contrast, there is no clear correlation between $^3\text{He}/^4\text{He}$ ratios and Mg numbers – either

for the Mascarene Islands data set as a whole or for the individual islands (Figure 2b). For example, olivines with Mg numbers between 83 and 84 have a wide range of $^3\text{He}/^4\text{He}$ ratios between 5.6 and 13.5 R_A . Gasparon et al. [1994] showed that low $^3\text{He}/^4\text{He}$ ratios of Sunda Arc lavas correlate with lower Mg numbers, i.e., more evolved lavas tend to have lower $^3\text{He}/^4\text{He}$ values. This was interpreted to reflect degassing during melt evolution, followed by crustal assimilation. However, the lowest $^3\text{He}/^4\text{He}$ ratios observed on Réunion, Mauritius and Rodrigues do not correspond to the lowest Mg values. Therefore, we suggest that post-eruptive radiogenic ingrowth of ^4He , from the alpha decay of groundmass U and Th, may have been implanted into the rims of olivine grains, thereby effectively lowering the $^3\text{He}/^4\text{He}$ values of olivines with low He contents. Since phenocrysts from Mauritius and Rodrigues islands are smaller in size and significantly older than those collected on Réunion Island, they may be more susceptible to addition of radiogenic helium; thus, irrespective of experimental precautions undertaken to minimize release of matrix-sited He (i.e., short crushing times [Hilton et al., 1993]), their measured $^3\text{He}/^4\text{He}$ ratios may represent minimum values.

4.2. Submarine Glasses From the Central Indian Ocean

4.2.1. Major and Trace Element Chemistry

[21] The majority of submarine basalts recovered from the CIR axis and the adjacent Gasitao, Three Magi, and Rodrigues ridges are tholeiitic, with some samples from the off-axis ridges having alkaline affinity. MgO and SiO₂ contents range from 6.6 to 14.4 wt % and from 44.7 to 51.8 wt %, respectively (Figure 3 and Table S1), and glasses from the off-axis volcanic structures generally have higher MgO and lower SiO₂ contents compared to on-axis samples (Figure 3). The high values of MgO observed in glasses recovered from the off-axis volcanic structures are not an effect caused by microphenocrysts of olivine. For example, the sample with the highest MgO content (14.4 wt %; D20–5 from the Gasitao Ridge) has less than 1% by volume of olivine present as phenocrysts of less than 0.5 mm in length, making a difference of no more than ~ 0.5 wt % MgO.

[22] Glasses from both the CIR axis and the off-axis ridges are characterized by a wide range in chondrite-normalized La/Sm ratios, $(\text{La}/\text{Sm})_N$, encompassing typical N-MORB-like ratios (<0.7 [Schilling et al., 1983]) through values as high as 2.09 and 1.74, respectively (Table 2). The highest $(\text{La}/\text{Sm})_N$ ratio (2.09) in this study is observed in sample RC1, which was collected from the western flank of the axial valley [Murton et al., 2005]. This sample also records high Ba/La and low Zr/Nb ratios of 11.1 and 8.3, respectively.

[23] We note that both Murton et al. [2005] and Nauret et al. [2006] previously concluded that the variations in incompatible element concentrations and ratios observed along the CIR axis must reflect the presence of a trace element enriched mantle source. Melting models fail to account for the observed variations in trace element characteristics [Murton et al., 2005], and the lack of a correlation between the Na₂O content (2.34 to 3.23 wt %) and bathymetry suggests that there are no systematic variations in the degree of partial melting along the CIR axis [Nauret et al., 2006]. One possible exception is sample RC1, the

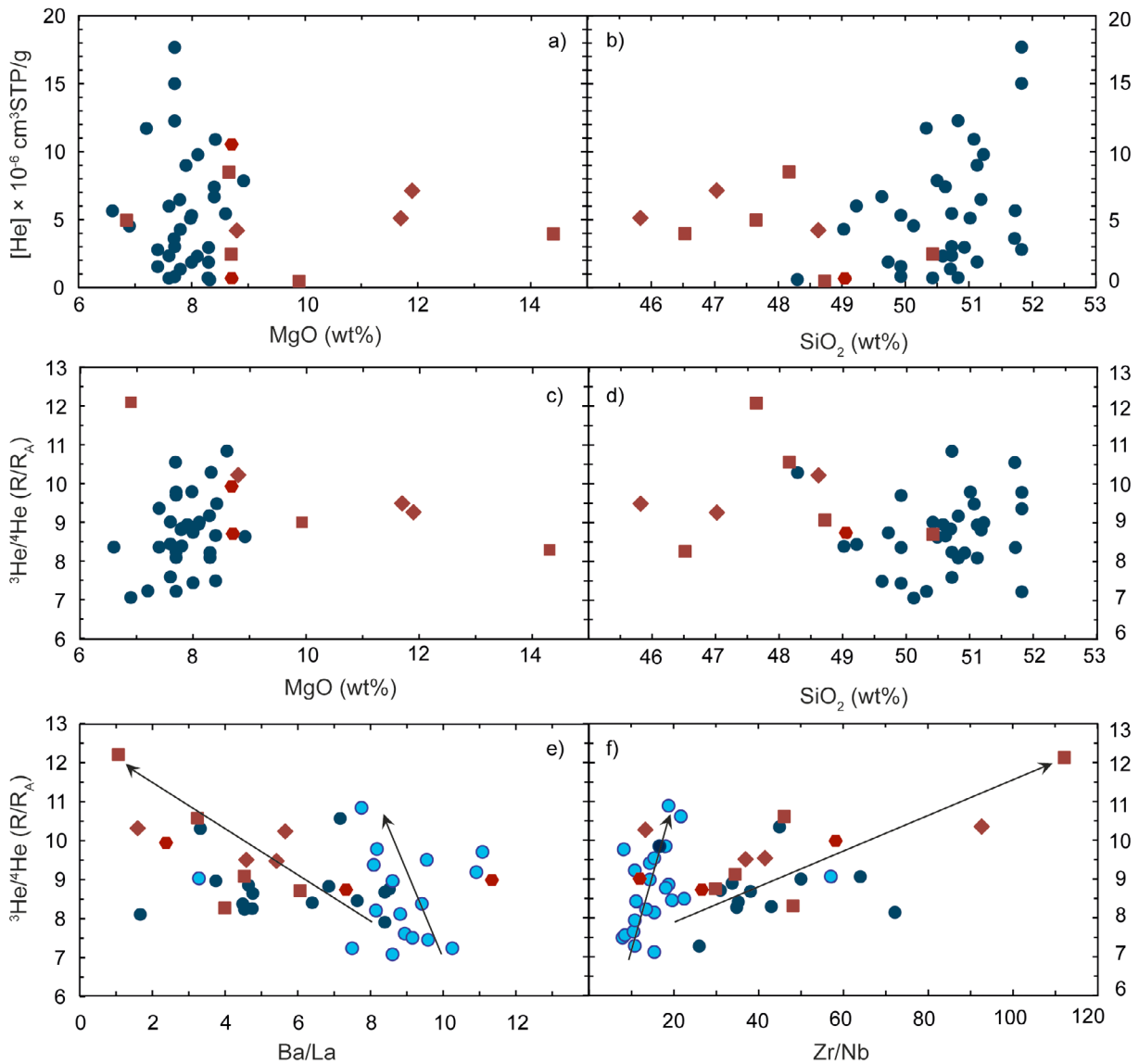


Figure 3. Helium concentrations of central Indian Ocean basalt glasses plotted against (a) MgO and (b) SiO₂ content in wt.%, as well as helium isotope ratios (³He/⁴He) plotted versus (c) MgO content, (d) SiO₂ content, (e) Ba/La, and (f) Zr/Nb ratios. Major and/or trace element data could not be obtained for some dredge locations with small sample yields. Symbols as in Figure 2; basaltic glasses collected between ~17° and 19.2°S along the ridge axis are shown in light blue in Figures 3e and 3f.

highly enriched ridge flank sample, which may be derived from a lower mean melt fraction generated at shallower depth of melting [Murton *et al.*, 2005]. Along the off-axis ridges, in contrast, incompatible trace element signatures may be affected by variations in the degree of partial melting.

4.2.2. Helium Abundances and Isotope Ratios

[24] Helium abundances in submarine glasses are extremely variable and range from 219 to 17,675 ($\times 10^{-9}$ cm³STP/g) (Table 2 and Figure 2a). Only sample D29–1 from the Rodrigues Ridge shows a significantly lower (air corrected) helium content of 2.2×10^{-9} cm³STP/g. Helium isotope ratios of the glass samples vary between 7.1 and 12.2 R_A

(Figure 2a), i.e., between values expected for depleted MORB mantle (8 ± 1 R_A [Graham, 2002]) and the helium isotope composition of lavas from Réunion Island with a mean value of 13.1 ± 0.7 R_A (see section 4.1). We note that duplicate analyses of samples DR08–1 and D22–1 show good reproducibility for helium isotopes (Table 2). In addition, samples D3–3 and D3–9 show ³He/⁴He ratios of 7.91 R_A and 7.96 R_A, respectively, illustrating that distinct pillow basalt fragments recovered in a particular dredge show homogeneous helium isotope compositions.

[25] A previous study reported He isotope ratios of 7.26 to 8.96 R_A for a series of four basalts from this region of the CIR, i.e., values that are undistinguishable from the range

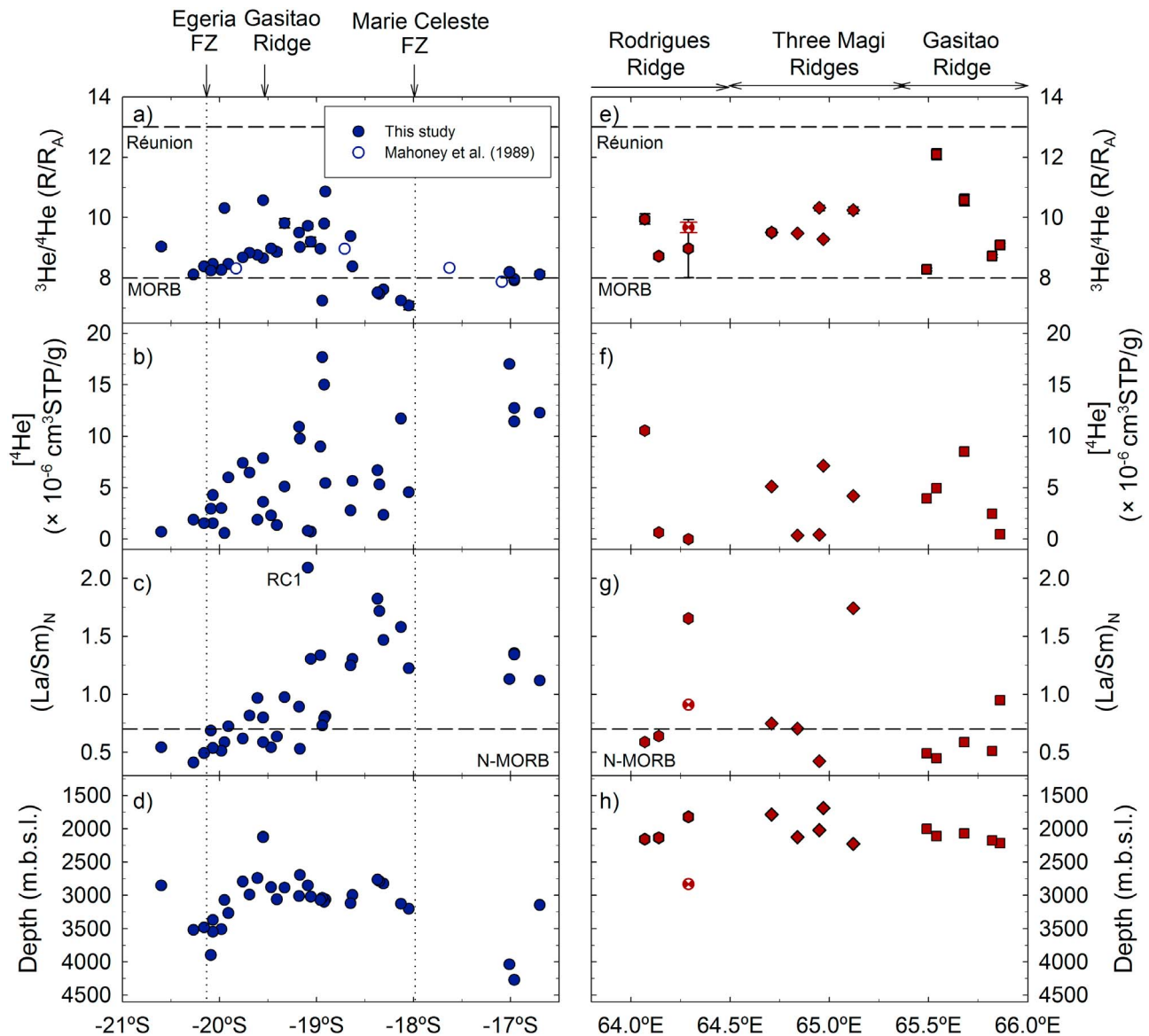


Figure 4. Helium isotope ratios ($^3\text{He}/^4\text{He}$), helium concentrations, chondrite-normalized La/Sm ($\text{La}/\text{Sm})_N$ ratios, and depth of sampling (in meters below sea level; mbsl) of submarine basalt glasses from the (a–d) CIR axis (as a function of latitude) and (e–h) off-axis volcanic structures (as a function of longitude). Also shown are the helium isotope ratios of four basalts obtained previously by *Mahoney et al.* [1989]. Helium isotope ratios for MORB mantle ($8 \pm 1 R_A$ [Graham, 2002]) and lavas from Réunion Island ($\sim 13.0 R_A$; this study), as well as the chondrite-normalized La/Sm ($\text{La}/\text{Sm})_N$ ratios for MORB (0.7 [Schilling et al., 1983]), are indicated by the horizontal dashed lines. Sample RC1 was collected from the edge of the axial valley [Murton et al., 2005]. Symbols as in Figure 2.

associated with normal MORB [Mahoney et al., 1989]. Our study reveals that most glasses recovered from the CIR axis have MORB-like $^3\text{He}/^4\text{He}$ ratios; however, 9 out of the 36 on-axis samples show helium isotope ratios $>9 R_A$ (i.e., 9.2 to $10.9 R_A$). The majority of glasses from the off-axis volcanic ridges (the Three Magi Ridges, the Gasitao Ridge, and the Rodrigues Ridge) have helium isotope ratios significantly greater than MORB values, i.e., 9 out of the 13 samples have $^3\text{He}/^4\text{He}$ ratios $>9 R_A$, and glass collected from an abyssal hill located ~ 40 km to the south of the Rodrigues Ridge also records an elevated helium isotope ratio of $9.7 R_A$. The highest $^3\text{He}/^4\text{He}$ ratio of $12.21 R_A$,

observed on the Gasitao Ridge, is indistinguishable from the helium isotope composition of olivine separates from Réunion (11.9 to $14.1 R_A$). We conclude that the high He isotope ratios of submarine glasses recovered between $\sim 19^\circ$ and 20°S require a contribution of helium derived from a high $^3\text{He}/^4\text{He}$ mantle source, consistent with input of hot spot mantle material from Réunion with a helium isotope composition of $13.1 \pm 0.7 R_A$ (see section 4.1).

[26] Figure 3 reveals that there is no clear correlation between either He abundances or isotopic compositions and the major element characteristics of basalts from this study. $^3\text{He}/^4\text{He}$ ratios, however, show a broad negative correlation

with Ba/La (Figure 3e) and a positive correlation with Zr/Nb ratios (Figure 3f). Furthermore, the majority of basaltic glasses collected between $\sim 17^\circ$ and 19.2°S along the ridge axis fall onto steeper trajectories than glasses sampled south of 19.2°S or along the off-axis volcanic structures; in other words, basalts from the northern part of the CIR axis generally have higher Ba/La (≥ 7 ; Figure 3e) and lower Zr/Nb (≤ 20 ; Figure 3f) ratios for a given $^3\text{He}/^4\text{He}$ value. Thus, our new data agree with previous studies [Murton *et al.*, 2005; Nauret *et al.*, 2006], which showed that basalts sampled near the Marie Celeste FZ are more enriched in incompatible trace elements than those collected further south.

4.2.3. Geographic Variations

[27] In Figure 4, we show the isotope composition and concentration of helium, as well as $(\text{La}/\text{Sm})_{\text{N}}$ ratios, for submarine glasses collected along the CIR axis and the off-axis volcanic ridges as a function of latitude and longitude, respectively, in order to evaluate the geographic variations in more detail. Figure 4a reveals that MORB-like $^3\text{He}/^4\text{He}$ ratios are observed in glasses recovered on the CIR axis in the vicinity of the Marie Celeste FZ, i.e., in the northern part of the study area. We note that a glass sample recovered from a near-ridge seamount south of the Marie Celeste FZ (sample D6–2) also records a low $^3\text{He}/^4\text{He}$ ratio of $7.2 R_{\text{A}}$ (Table 2 and Figure 2a), indistinguishable from the values observed on the adjacent segment of the ridge axis. Along the ridge axis to the south, there is a marked increase in $^3\text{He}/^4\text{He}$, to values $>10 R_{\text{A}}$ between $\sim 19^\circ$ and 20°S , before ratios return to $\sim 8 R_{\text{A}}$ close to the Egeria FZ. The glasses from the southern part of the ridge, characterized by low $^3\text{He}/^4\text{He}$ ratios, show low He concentrations ($\leq 5 \times 10^{-6} \text{ cm}^3\text{STP/g}$) and $(\text{La}/\text{Sm})_{\text{N}}$ ratios (< 0.7), as well as the lowest Ba/La, and highest Zr/Nb ratios (Figures 3e and 3f). Overall, however, $^3\text{He}/^4\text{He}$ values do not correlate with helium concentrations (Figures 2a and 4b) or $(\text{La}/\text{Sm})_{\text{N}}$ ratios (Figure 4c) along the CIR. The highest He abundances ($>10 \times 10^{-6} \text{ cm}^3\text{STP/g}$) are measured in glasses collected to the north of the Marie Celeste FZ and in the central part of the studied ridge segment (Figure 4b). In contrast, the highest $(\text{La}/\text{Sm})_{\text{N}}$ and Ba/La values, as well as low Zr/Nb ratios, characteristic of an enriched mantle component, are observed immediately south of the Marie Celeste FZ (Figure 4c) where $^3\text{He}/^4\text{He}$ ratios are the lowest (Figure 4a).

[28] Along the Rodrigues, Three Magi, and Gasitao ridges, there are no systematic variations in $^3\text{He}/^4\text{He}$ ratios and He concentrations as the CIR axis is approached. Helium isotope ratios range from 8.7 to $12.2 R_{\text{A}}$ at the Gasitao Ridge, i.e., the volcanic ridge closest to the CIR, whereas the Three Magi and Rodrigues ridges show $^3\text{He}/^4\text{He}$ ratios of 9.5 to $10.3 R_{\text{A}}$ and 8.7 to $9.9 R_{\text{A}}$, respectively (Figure 4e). Helium abundances are highly variable from east to west, with glasses from each individual volcanic ridge recording a wide range in helium concentrations (Figure 4f).

[29] Mellor [1998] showed that basalts recovered from the Rodrigues Ridge (i.e., between 60°E and 64.5°E) record a decrease in average $(\text{La}/\text{Sm})_{\text{N}}$ ratios from 3.87 to 0.95 with increasing distance from Réunion Island. Our new $(\text{La}/\text{Sm})_{\text{N}}$ data for glasses sampled between 64°E and 66°E agree with the previously observed trend (Figure 6a), i.e., the majority of glasses collected along the Rodrigues, Three Magi, and Gasitao ridges have $(\text{La}/\text{Sm})_{\text{N}}$ ratios < 1 . While two samples

from the Three Magi and Rodrigues ridges show significantly higher $(\text{La}/\text{Sm})_{\text{N}}$ ratios of 1.74 and 1.65 , respectively (Figure 4g), these trace element ratios still fall in the range of values observed at individual dredge sites by Mellor [1998] (Figure 6a). We note that the distinct trace element signatures of these two samples do not correlate with anomalous helium isotope ratios or abundances; however, their $^3\text{He}/^4\text{He}$ ratios may have been modified by post-eruptive ^4He ingrowth, a process that will be discussed in section 5.1.1.

5. Discussion

[30] Our helium isotope survey reveals that submarine glasses recovered from the CIR record a range in $^3\text{He}/^4\text{He}$ ratios, between values expected for depleted MORB mantle and the helium isotope compositions observed in lavas from Réunion Island. Glasses sampled both to the north of the Marie Celeste FZ and to the south of the Egeria FZ show $^3\text{He}/^4\text{He}$ ratio that are undistinguishable from the range associated with normal MORB. However, a high $^3\text{He}/^4\text{He}$ ratio component is present in the subridge mantle between $\sim 19^\circ$ and 20°S , as well as in the mantle beneath the off-axis volcanic ridges to the west of the CIR. As the focus of this study is to identify the mantle end-member helium systematics, and to understand the dynamics of mantle mixing in this region, we first define the intrinsic helium characteristics of the different mantle sources by evaluating other mechanisms capable of modifying the volatile inventory of submarine basalts. While pillow basalts recovered from the off-axis structures are older and in part manganese-encrusted, the “zero age” of lavas erupted along the CIR axis renders any post-eruptive ingrowth of ^4He insignificant. However, shallow level magmatic processes and pre-eruptive radiogenic ^4He ingrowth are considered in this section.

5.1. Effects of Shallow Level Magmatic Processes

5.1.1. Off-Axis Glasses: Post-eruptive ^4He Ingrowth

[31] In the case of post-eruptive ingrowth, $^3\text{He}/^4\text{He}$ ratios can be lowered over time by the addition of ^4He from the decay of U and Th. Therefore, it is important to evaluate the effect of radiogenic He production on the $^3\text{He}/^4\text{He}$ values of glasses from the off-axis volcanic ridges which may not be zero age. Dredged lavas from the Rodrigues Ridge range in age from 8 to 10 Ma [Duncan *et al.*, 1990], whereas samples from the easternmost Gasitao Ridge provide ages of 0.4 and 1.8 Ma [Dyment *et al.*, 2001]. The maximum amount of radiogenic ^4He produced over time in basalts erupted off axis can be estimated according to [Graham *et al.*, 1987]

$$^4\text{He}^* = 2.80 \times 10^{-8} [\text{U}] (4.35 + \text{Th}/\text{U}) T (\text{cm}^3\text{STP/g}) \quad (1)$$

where T is the time in Ma, and $[\text{U}]$ and Th/U are the uranium concentration in ppm and the atomic ratio, respectively, measured in the glasses (see Table S2 and Nauret *et al.* [2006]). For samples from the Gasitao Ridge, the radiogenic ^4He production is of the order of ~ 2 to 17 ($\times 10^{-9} \text{ cm}^3\text{STP/g}$). Under the unlikely condition of complete transfer of $^4\text{He}^*$ from the glass matrix (where it is produced) to the vesicle phase, post-eruptive ^4He ingrowth may have modified the helium isotope composition of sample D18–2, which shows the highest $[\text{U}]$ and lowest $[^4\text{He}]$. For this

sample, the amount of radiogenic ^4He produced in 1.8 Ma is $\sim 4\%$ of the total helium abundance, and the initial $^3\text{He}/^4\text{He}$ ratio may have been 9.4 R_A : marginally higher than the ratio of 9.1 R_A measured today. In contrast, ~ 20 to 100 ($\times 10^{-9}$ $\text{cm}^3\text{STP}^4\text{He}^*/\text{g}$) may have been produced in the 8 to 10 Ma old basalts from the Rodrigues Ridge based on their U and Th content (given in Table S2). Thus, post-eruptive ^4He ingrowth may have modified the initial $^3\text{He}/^4\text{He}$ ratio of the He-poor samples D29–1 and D34–1, and the $^3\text{He}/^4\text{He}$ ratios of 9.0 and 8.7 R_A measured in these glasses today may represent minimum values. Consequently, if the total $^4\text{He}^*$ was transferred from the glass matrix to the vesicles, the helium isotope ratios of the samples from the Rodrigues Ridge may have been significantly higher than typical MORB values (e.g., up to $\sim 10.3 R_A$ in sample D34–1).

5.1.2. On-Axis Glasses: Degassing

[32] Degassing plays an important role in the helium inventory of any oceanic basalt [Bottinga and Javoy, 1990; Marty and Zimmermann, 1999; Hilton et al., 2000; Moreira and Sarda, 2000]. Virtually all oceanic basalts are supersaturated with respect to CO_2 (the carrier of magmatic helium) when they erupt, resulting in the formation of CO_2 -rich gas bubbles and loss of helium from the melt phase [Sarda and Graham, 1990]. Since the solubility of CO_2 decreases as the confining pressure decreases [Dixon et al., 1995; Jendrzejewski et al., 1997], basaltic melts erupting at shallow water depths (i.e., under low hydrostatic pressures) will lose a higher proportion of their primary volatile inventory. In addition, the solubility of CO_2 is controlled by the water content of the magma; for example, an increase in the water content of a basaltic melt from ~ 0.2 to 1 wt % H_2O (at 200 bar) would decrease the CO_2 solubility from 100 to 50 ppm [Dixon et al., 1995]. Thus, a water-rich magma will lose its dissolved CO_2 more efficiently than an anhydrous melt. Consequently, a combination of high water contents and shallow eruption depths will promote extensive degassing, and a lower concentration of helium is to be expected for a melt erupting under such conditions.

[33] We recovered submarine glasses from the CIR axis between 2120 and 4270 m water depths (Table 2 and Figure 4d). Figure 4d illustrates that between the Marie Celeste and the Egeria FZ, the depth of the CIR is greatest in the south. In addition, Murton et al. [2005] noted that water concentrations (determined for a subset of samples by Fourier transform infrared laser spectroscopy) and $\text{H}_2\text{O}/\text{TiO}_2$ ratios of basaltic glasses decrease from 0.49 to 0.11% and 0.41 to 0.09, respectively, southward along the ridge axis. Thus, due to a greater confining pressure at eruption and low water concentrations, the melts from the southern end of the CIR segment are expected to retain their primary helium inventory more efficiently. However, our data reveal that the helium contents of glasses collected near the Egeria FZ are the lowest (Figure 4b). In addition, helium abundances are highly variable for a given water depth. These observations lead us to conclude that the confining (i.e., hydrostatic) pressure and/or the water content are not the major controls on the observed variations in helium abundances of CIR basalts.

[34] Alternatively, fractional crystallization in a shallow magma chamber may increase the extent of gas loss from a melt [Marty and Zimmermann, 1999; Burnard et al., 2002]. Since volatiles (e.g., He and CO_2) are expected to behave

incompatibly, their effective concentrations in a melt increase during fractional crystallization and eventually exceed the solubility limits at the magma chamber pressure. Thus, as CO_2 -rich bubbles form and other volatile species partition between the melt and the vapor phase, magmas are depleted in mantle-derived volatiles. Therefore, helium abundances are expected to correlate with a crystal fractionation index (e.g., the MgO content) if the extent of crystallization was the main control on the volatile solubility [Hilton et al., 1993]. However, Figure 3 shows that the helium abundances of our sample set do not show a clear decrease with decreasing MgO content, that is, with increasing fractional crystallization. On-axis samples are characterized by highly variable helium concentrations for a relatively restricted range (6.6 to 8.9 wt %) of MgO contents. This suggests that the observed variations in helium abundances along the CIR axis cannot be explained by varying degrees of fractional crystallization alone.

[35] We conclude that shallow level magmatic processes can be ruled out as the major controls on the wide helium concentration contrasts observed in basalts collected along the CIR axis. However, a more detailed evaluation of the degree of degassing requires knowledge of H_2O and CO_2 concentrations. Major volatile content (H_2O and CO_2) measurements by secondary ion mass spectrometry (SIMS) on all glass samples from the KNOX11RR cruise are in progress. These data will allow a more quantitative evaluation of the relationship between major volatile abundances and helium concentrations, and the results will be discussed in a separate publication (P. H. Barry et al., manuscript in preparation, 2011). Here, we propose that the helium systematics of on-axis basalts are the result of mixing between different mantle sources with distinct helium inventories. Next, we discuss the helium characteristics of these different mantle components.

5.2. Enriched Mantle at $\sim 18^\circ\text{S}$: Preeruptive ^4He Ingrowth

[36] The highest $(\text{La}/\text{Sm})_N$ ratios along the CIR axis, characteristic of an enriched mantle source for a given degree of melting, are observed in basaltic glasses collected immediately south of the Marie Celeste FZ. These samples also show the highest ratios of other incompatible elements, e.g., Ba/La and Nb/Zr. However, glasses from this region show the lowest $^3\text{He}/^4\text{He}$ ratios ($< 8 R_A$), and their Sr–Nd–Pb isotope characteristics differ from the composition of lavas presently erupting on Réunion [Nauret et al., 2006]. Consequently, the trace element enriched mantle material cannot be supplied by direct influx from Réunion toward the CIR. As an alternative explanation, we evaluate if on-axis melts in this region may be sampling (1) a “fossil” Réunion hot spot mantle component or (2) metasomatized (i.e., trace element enriched) MORB-like mantle.

5.2.1. “Fossil” Réunion Hot Spot Mantle

[37] Basalts recovered along the Réunion hot spot track (between the Deccan flood basalts in India and Réunion Island) during Ocean Drilling Program (ODP) Leg 115 record a clear increase in $^{87}\text{Sr}/^{86}\text{Sr}$ and $^{206}\text{Pb}/^{204}\text{Pb}$ ratios, as well as a decrease in ϵNd values with time [Fisk et al., 1989; White et al., 1990]. These compositional changes have been attributed to temporal variations in the degree of mixing between the upwelling Réunion hot spot mantle and shallower asthenospheric MORB mantle [Duncan et al., 1990;

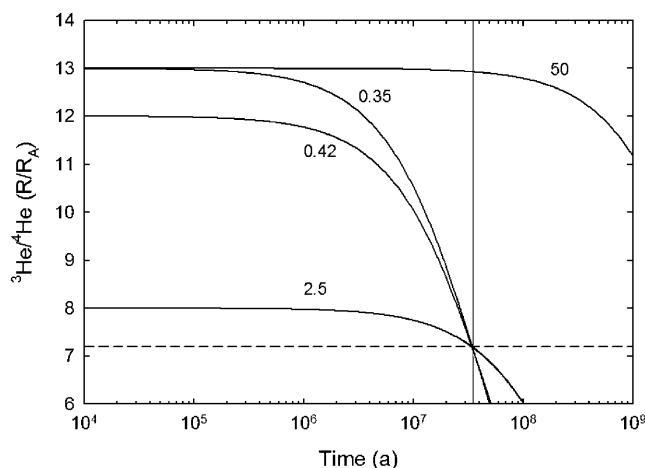


Figure 5. Predicted time-dependent evolution of the ${}^3\text{He}/{}^4\text{He}$ ratio (R/R_A) of a “fossil” Réunion mantle component due to radiogenic ${}^4\text{He}$ ingrowth from decay of U and Th over 34 Ma. Curves are modeled for a mantle reservoir with $[\text{U}] = 35$ ppb, $\text{Th}/\text{U} = 3.9$, a ${}^4\text{He}$ production ratio of $2.32 \times 10^{-7} \text{ cm}^3\text{STP/ppm U/Ma}$ [Ozima and Podosek, 2002], and an initial He composition of $13 R_A$ and $50 \times 10^{-6} \text{ cm}^3\text{STP}^4\text{He/g}$, $13 R_A$ and $0.35 \times 10^{-6} \text{ cm}^3\text{STP}^4\text{He/g}$, $12 R_A$ and $0.42 \times 10^{-6} \text{ cm}^3\text{STP}^4\text{He/g}$, and $8 R_A$ and $2.5 \times 10^{-6} \text{ cm}^3\text{STP}^4\text{He/g}$. The horizontal dashed line indicates the helium isotope ratio observed in CIR glasses near the Marie Celeste FZ, i.e., ${}^3\text{He}/{}^4\text{He} = 7.2 R_A$. See section 5.2.1 for details.

White et al., 1990]. As the CIR was located closer to the Réunion hot spot in the past, the higher temperature and lower viscosity and density regime associated with the spreading ridge resulted in enhanced entrainment of depleted MORB mantle by the ascending hot spot material. In this respect, studies of other hot spots located close to spreading ridges (e.g., Iceland, Bouvet, Galápagos, and Easter) have revealed that the isotope characteristics of OIB lavas show mixing trends with MORB-like mantle [Hanan and Schilling, 1989; Hauri et al., 1994]. Thus, as the Réunion hot spot was centered under the CIR, mixing of the two mantle components could have generated basalts with lower ${}^{87}\text{Sr}/{}^{86}\text{Sr}$ and ${}^{206}\text{Pb}/{}^{204}\text{Pb}$ ratios, as well as higher ϵNd values compared to lavas presently erupting on Réunion [Duncan et al., 1990; White et al., 1990]. These trace element and Sr-Nd-Pb isotope characteristics resemble the composition of basalts presently erupting near the Marie Celeste FZ, i.e., at the northern end of the studied CIR segment [Nauret et al., 2006]. If a “fossil” Réunion hot spot component is still present in the mantle beneath the CIR, it must have been isolated from mixing with ambient MORB-like mantle over the past 34 Ma in order to retain a distinct trace element and Sr-Nd-Pb isotope composition; however, radiogenic ${}^4\text{He}$ ingrowth from the decay of U and Th will have modified the initial ${}^3\text{He}/{}^4\text{He}$ ratio.

[38] In order to evaluate if a “fossil” Réunion mantle component represents a suitable end-member for the helium characteristics of basalts collected near the Marie Celeste FZ, the He and (U+Th) content of this reservoir need to be estimated. Vlastèlic et al. [2006] showed that the Réunion hot spot source has preserved a Th/U ratio of 3.9, similar to

the bulk Earth value [Rocholl and Jochum, 1993] and identical to the Th/U ratio measured in sample D9–1 collected in the vicinity of the Marie Celeste FZ. Assuming 10% partial melting in the subridge mantle and quantitative partitioning of uranium from the solid phase into the melt, we estimate a uranium concentration of 35 ppb for the mantle source on the basis of the uranium content of sample D9–1 ($[\text{U}] = 0.35$ ppm). Therefore, we adopt values of $[\text{U}] = 35$ ppb, $\text{Th}/\text{U} = 3.9$, and a corresponding ${}^4\text{He}$ production ratio of $2.33 \times 10^{-7} \text{ cm}^3\text{STP/ppm U/Ma}$ [Ozima and Podosek, 2002], and we assume an initial ${}^3\text{He}/{}^4\text{He}$ ratio of $13.0 R_A$ (i.e., the helium isotope composition of lavas presently sampled on Réunion Island). The helium content of the Réunion hot spot component, however, is difficult to constrain. The primary helium content of different mantle reservoirs cannot be determined through direct measurements of volcanic materials, and models predict a wide range of ${}^4\text{He}$ concentrations between ~ 0.5 to $50 \times 10^{-6} \text{ cm}^3\text{STP}^4\text{He/g}$ for the OIB mantle source [e.g., Porcelli and Ballentine, 2002; van Keken et al., 2002]. The highest source estimates are based on steady state, layered mantle models, with the assumption that the lower mantle represents the source of OIB and has remained a closed system over Earth history [Porcelli and Wasserburg, 1995]. In contrast, significantly lower OIB source estimates are derived from studies of ${}^3\text{He}$ and magma flux rates at Kilauea [Hilton et al., 1997]. Consequently, we evaluate the effect of radiogenic ${}^4\text{He}$ ingrowth for a range of helium concentrations.

[39] Figure 5 shows that for an initial helium concentration of $50 \times 10^{-6} \text{ cm}^3\text{STP}^4\text{He/g}$, the helium isotope ratio in the mantle source would decrease by only $\sim 0.5\%$ after 34 Ma of radiogenic ${}^4\text{He}$ ingrowth in a closed system. In order to shift the ${}^3\text{He}/{}^4\text{He}$ ratio to a value of $7.2 R_A$, i.e., the ratio observed in basalts collected near the Marie Celeste FZ today, a significantly lower initial helium content of $\sim 0.35 \times 10^{-6} \text{ cm}^3\text{STP}^4\text{He/g}$ is required. However, the “fossil” Réunion mantle at 34 Ma may have had a different He isotope composition from the present value; enhanced entrainment of depleted MORB mantle by the ascending hot spot material in the past may have resulted in a lower helium isotope ratio of the trace element enriched mantle component compared to lavas currently erupting on Réunion. In this respect, we note that Older Series (5 to 8 Ma) lavas on Mauritius, located on the former site of the Réunion hot spot, have ${}^3\text{He}/{}^4\text{He}$ ratios of only ~ 8 to $11.8 R_A$ (this study and Hanyu et al. [2001]), consistent with a higher proportion of helium derived from a MORB-like reservoir. Nonetheless, an enriched mantle component with a lower initial ${}^3\text{He}/{}^4\text{He}$ ratio of ~ 8 to $12 R_A$ also requires a low primary helium content (i.e., 0.4 to $2.5 \times 10^{-6} \text{ cm}^3\text{STP}^4\text{He/g}$) for a decrease of the helium isotope composition to a value of $\sim 7.2 R_A$ by radiogenic ingrowth over 34 Ma.

[40] These evaluations illustrate that the helium characteristics of glasses collected south of the Marie Celeste FZ can be explained by closed system radiogenic ${}^4\text{He}$ ingrowth in a “fossil” Réunion mantle component. However, the helium concentration in this mantle reservoir must be extremely low, i.e., comparable to the lowest concentration estimates for the OIB source and even lower than estimates for the MORB source (~ 4 to $15 \times 10^{-6} \text{ cm}^3\text{STP}^4\text{He/g}$ [Porcelli and Ballentine, 2002]). In this scenario, this may either indicate that the Réunion hot spot source is charac-

terized by a low intrinsic helium inventory or, alternatively, that significant degassing occurred during or after ascent of the upwelling hot spot material into the shallower mantle region. We note that the strong helium depletion observed in many OIB samples has been explained by extensive near-surface degassing [e.g., Hilton *et al.*, 1997; Hilton *et al.*, 2000; Gonnermann and Mukhopadhyay, 2007]; a corollary of these models is that the He content of the high $^3\text{He}/^4\text{He}$ ratio OIB source may be similar to, or greater than the concentration in the MORB source.

5.2.2. Metasomatized MORB Mantle

[41] Alternatively, Nauret *et al.* [2006] and Hémond *et al.* [2006] suggested that lavas collected near the Marie Celeste FZ may be derived from fertilized MORB-like mantle, as recently suggested for enriched basalts from the mid-Atlantic Ridge south of the Kane FZ. Donnelly *et al.* [2004] suggested that the generation of enriched MORB (E-MORB) requires two stages: depleted upper mantle is first fertilized (i.e., enriched in incompatible trace elements) by low-degree melts at subduction zones; the metasomatized mantle is then recycled to mid-ocean ridges where it is melted to greater extent to form E-MORB. Furthermore, they concluded that convective mantle mixing occurs on a timescale of ~ 300 Ma, comparable to the stirring times proposed for the upper mantle by Allègre *et al.* [1995] on the basis of helium isotope ratios observed in MORB.

[42] For this scenario, we assume that the E-MORB reservoir is initially characterized by a helium isotope composition expected for normal MORB mantle ($8 \pm 1 R_A$ [Graham, 2002]). During convective transport of the fertilized mantle component to the ridge, radiogenic ingrowth of ^4He lowers the $^3\text{He}/^4\text{He}$ ratio. Adopting the U-Th characteristics discussed in the section 5.2.1 (i.e., $[U] = 35$ ppb, $\text{Th}/\text{U} = 3.9$, and a ^4He production ratio of $2.33 \times 10^{-7} \text{ cm}^3\text{STP/ppm U/Ma}$ [Ozima and Podosek, 2002]), we calculate a radiogenic ^4He contribution of $2.4 \times 10^{-6} \text{ cm}^3\text{STP}^4\text{He/g}$ in 300 Ma. Thus, for MORB mantle with an initial helium concentration of 4 to $15 \times 10^{-6} \text{ cm}^3\text{STP}^4\text{He/g}$ [Porcelli and Ballentine, 2002] and a helium isotope composition of $8 R_A$, the $^3\text{He}/^4\text{He}$ ratio will decrease to between 5.0 and $6.9 R_A$. These values are comparable to, yet slightly lower than, the ratios observed in glasses near the Marie Celeste FZ.

[43] In summary, we conclude that the helium characteristics of basalts sampled near the Marie Celeste FZ can be explained by either melting of a “fossil” Réunion hot spot mantle component or fertilized MORB mantle; in either case, the initial He isotope composition has been modified by preruptive ingrowth of radiogenic ^4He over time. However, we caution that both models are critically dependent on estimates of the He and (U+Th) characteristics of the source mantle, as well as the degree of partial melting. Furthermore, mantle stirring timescales, here assumed to be of the order of ~ 300 Ma, are not well constrained. We note that a companion study will investigate the relationship between He and other isotope systems (e.g., Sr, Nd, and Pb); the radiogenic isotope characteristics of the basaltic glasses will provide additional constraints on the origin of the trace element enriched mantle component in the northern part of the studied CIR segment (C. Hémond *et al.*, manuscript in preparation, 2011). Nonetheless, we emphasize that the trace element enriched, low $^3\text{He}/^4\text{He}$ ratio mantle component is only observed in the vicinity of the Marie Celeste FZ; lavas

erupting near the Egeria FZ, ~ 150 km to the south, record normal MORB-like trace element and helium characteristics. Thus, these observations call for a mechanism whereby distinct, small-scale heterogeneities can remain isolated in the ambient shallow mantle for 10s to 100s of Ma until they are sampled at the ridge axis.

5.3. Interaction of the CIR With the Réunion Hot Spot

[44] Our helium isotope survey reveals that $^3\text{He}/^4\text{He}$ ratios significantly greater than MORB values are observed between $\sim 19^\circ$ and 20°S along the CIR axis (Table 2 and Figure 4), i.e., close to the present-day intersection of the CIR and the off-axis volcanic structures. Furthermore, high He isotope values up to $12.2 R_A$ along the Gasitao Ridge, the Three Magi Ridges, and the east-west oriented Rodrigues Ridge show that a high $^3\text{He}/^4\text{He}$ ratio component is present beneath these volcanic ridges to the west of the CIR axis. Thus, our data appear consistent with influx of an eastward flowing tongue of high $^3\text{He}/^4\text{He}$ mantle material from the Réunion hot spot into the subridge mantle of the CIR, along an eastward trajectory that impinges the ridge at $\sim 19.5^\circ\text{S}$.

[45] Morgan [1978] suggested that in the case of off-axis hot spots, a pipe-like flow from the hot spot to the adjacent mid-ocean ridge axis may develop. As the ridge migrates away from the initially ridge-centered hot spot, it is continuously fed by preferential flow of enriched mantle material along a thermally induced sublithospheric channel [Schilling, 1985; Schilling, 1991; Kincaid *et al.*, 1995]. Flow along the channel can be sustained for hot spot–ridge separations up to ~ 1400 km, whereas greater distances appear to inhibit interaction due to increased fluid viscosities caused by cooling along the flow path [Schilling, 1985, 1991; Kincaid *et al.*, 1995]. At the intersection of the sublithospheric channel and the ridge axis, enhanced volcanism generates seamounts and islands which eventually form ridge-perpendicular volcanic ridges on the oceanic plate as it is moving away from the ridge [Morgan, 1978]. In this scenario, the off-axis volcanic ridges will have the same age as the underlying crust, i.e., their ages will increase with increasing distance from the ridge axis. However, Duncan *et al.* [1990] noted that the entire Rodrigues Ridge formed at 8 to 10 Ma without a westward age progression, and the Gasitao Ridge also appears to be younger than the underlying crust [Dyment *et al.*, 2001]. These observations are inconsistent with the notion of generation of volcanic lineaments to the west of the CIR by a pipe-like channel supplying hot spot mantle material to the ridge axis.

[46] Therefore, Dyment *et al.* [2001] proposed that the Rodrigues Ridge, the Three Magi Ridges, and the Gasitao Ridge result from filling of tensional cracks in the lithosphere. Mittelstaedt and Ito [2005] showed that mantle upwelling at an off-axis hot spot influences the lithospheric stress field between the hot spot and the nearby spreading ridge, resulting in the formation of volcanic lineaments along areas of high integrated tension. Thus, the volcanic ridges to the west of the CIR axis do not require a pipe-like sublithospheric channel, and upwelling Réunion hot spot mantle may be expanding outward as a broad, pancake-like gravity current along the base of the lithosphere [Ito *et al.*, 1997; Albers and Christensen, 2001].

[47] Since the thickness of oceanic lithosphere increases as the square root of its age [Parker and Oldenburg, 1973],

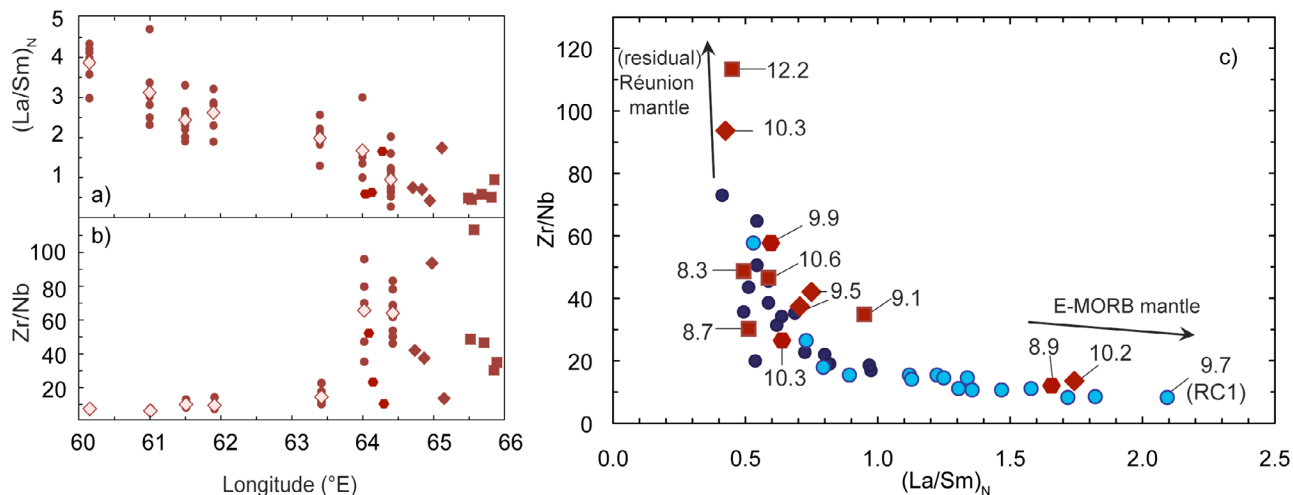


Figure 6. Trace element ratios (a) $(La/Sm)_N$ and (b) Zr/Nb ratios as a function of longitude for central Indian Ocean basalt glasses from this study and seven dredge sites along the Rodrigues Ridge from Mellor [1998] (filled circles are individual lava samples; open diamonds are average values). (c) Plot of Zr/Nb versus $(La/Sm)_N$ ratios of samples from this study. Helium isotope ratios (in the form of R/R_A) are shown for glass samples from the off-axis volcanic structures and sample RC1, which was collected from the western flank of the axial valley [Murton *et al.*, 2005]. High $(La/Sm)_N$ and low Zr/Nb ratios observed in samples collected north of $19.2^{\circ}S$ along the CIR axis (shown in light blue) likely reflect the presence of a trace element enriched mantle component (E-MORB) near the Marie Celeste FZ (sections 5.2.1 and 5.2.2), whereas sample RC1 may be derived from a lower mean melt fraction [Murton *et al.*, 2005]. The depleted trace element pattern and concomitant helium isotope enrichment (i.e., high $^3He/^4He$ ratios) of samples from the off-axis volcanic structures reflects the presence of (residual) Réunion hot spot mantle material, which has lower $(La/Sm)_N$ and higher Zr/Nb ratios than generally observed for an “enriched” mantle source. This is likely due to previous depletion in trace elements by melt extraction along the flow path toward the CIR.

thinning of the lithosphere toward the CIR axis may provide the gravitational driving force that causes the expanding Réunion hot spot mantle to flow “upslope” toward the ridge axis [Kincaid *et al.*, 1995, 1996; Sleep, 1996]. In this case, shallowing of the base of the lithosphere, combined with additional thinning induced by tension, will trigger decompression melting along the flow path of the hot spot material [Sleep, 1996], and continuous melt extraction processes are expected to progressively deplete the expanding Réunion hot spot mantle material in incompatible elements as it migrates toward the subridge region of the CIR. In this respect, Mellor [1998] previously showed that basalts from the Rodrigues Ridge record a decrease in average $(La/Sm)_N$ ratios from 3.87 to 0.95 and a concomitant increase in Zr/Nb ratios, from 6.3 to 65.7, with increasing distance from Réunion Island (Figures 6a and 6b), consistent with the notion that the Réunion mantle component is progressively depleted in incompatible trace elements along its flow path. However, superimposed on the general geochemical gradients from west to east, lavas collected at an individual dredge site record a wide range in trace element signatures [Mellor, 1998], possibly reflecting small-scale source heterogeneities, mixing of different mantle components, and/or variations in the degree of melting and fractional crystallization.

[48] Our study reveals that some domains of the expanding hot spot mantle must retain their intrinsic helium isotope characteristics, as evidenced by $^3He/^4He$ ratios as high as 12.2 R_A at the Gasitao Ridge, ~ 1000 km away from the Réunion hot spot. Notably, the basaltic glass sample with

the highest $^3He/^4He$ value (12.2 R_A ; DR08–1) showed the highest $^{87}Sr/^{86}Sr$ (0.7040) and one of the lowest $^{143}Nd/^{144}Nd$ ratios (0.5129) in the study of Nauret *et al.* [2006], i.e., a radiogenic isotope signature that is similar to the Réunion hot spot source [e.g., Luais, 2004; Bosch *et al.*, 2008; Pietruszka *et al.*, 2009]. In contrast, the same sample records the lowest Ba/La (1.1) and highest Zr/Nb (113.3) ratios, as well as a low $(La/Sm)_N$ value of 0.45 (Table 2 and Figures 3 and 6c); these trace element characteristics are typically attributed to melting of normal MORB mantle [e.g., Sun and McDonough, 1989; Albarède *et al.*, 1997; Le Roux *et al.*, 2002]. We propose that the isotope enrichment (i.e., high $^3He/^4He$ and $^{87}Sr/^{86}Sr$ together with low $^{143}Nd/^{144}Nd$ ratios) and concomitant trace element depletion observed at the Gasitao Ridge results from partial melting of a mantle source that has been contaminated by Réunion hot spot mantle; in this case, the hot spot component is characterized by significantly lower $(La/Sm)_N$ and Ba/La ratios, as well as a higher Zr/Nb value, than generally observed for “enriched” hot spot mantle as a result of previous extraction of incompatible trace elements by melting (Figure 6). These geochemical characteristics are also observed in basaltic glasses sampled on the CIR axis at $\sim 19.5^{\circ}S$; i.e., where the eastward flowing tongue of Réunion hot spot material impinges the ridge, basalts are characterized by $^3He/^4He$ values up to 10.6 R_A and typical N-MORB-like trace element ratios (Figures 3e, 3f, 4c).

[49] While some basaltic glasses from the Gasitao Ridge show the high $^3He/^4He$ signature of the Réunion mantle, the

helium isotope ratios along the Rodrigues, Three Magi, and Gasitao ridges are highly variable, with glasses from each individual volcanic ridge showing a range in $^3\text{He}/^4\text{He}$ values (Figures 4e and 4g). In contrast to the trace element characteristics, the helium and Sr-Nd-Pb isotope signatures of the hot spot component cannot be altered by melt removal alone. Therefore, *Nauret et al.* [2006] previously concluded that the decrease in $^{87}\text{Sr}/^{86}\text{Sr}$ and $^{206}\text{Pb}/^{204}\text{Pb}$ ratios, and concomitant increase in $^{143}\text{Nd}/^{144}\text{Nd}$ observed in their study along the Gasitao Ridge requires mixing of Réunion hot spot material with MORB-like mantle, and *Sheth et al.* [2003] and *Nohda et al.* [2005] proposed a similar scenario to explain the variations in Sr-Nd-Pb isotope compositions observed in Older Series, Intermediate Series, and Younger Series lavas from Mauritius. Furthermore, Intermediate series and Younger Series lavas from Mauritius and Rodrigues show $^3\text{He}/^4\text{He}$ ratios of 6.5 to 8.4 R_A [*Hanyu et al.*, 2001]. These helium isotope signatures suggest that the late-stage lavas are derived from a mantle source that is dominated by a MORB-like component, and they rule out melting of a heterogeneous “plum pudding” Réunion mantle component alone as the source of lavas in Mauritius [*Paul et al.*, 2005, 2007]. Consequently, we propose that the variations in $^3\text{He}/^4\text{He}$ ratios of glasses recovered along the off-axis volcanic structures can only be explained by mixing of the (residual) hot spot component with partial melts derived from a MORB-like mantle reservoir. In this case, the observed helium isotope ratios will be controlled by the helium concentrations of each end-member. For example, mixing a small proportion of a ^3He -rich mantle component with a depleted mantle end-member will significantly change the $^3\text{He}/^4\text{He}$ ratio without concomitantly modifying the trace element signature. Along the off-axis volcanic ridges to the west of the CIR, variations in the degree of previous melt removal and degassing along the flow path of the hot spot mantle material may result in significant spatial heterogeneities in the helium contents of both the residual Réunion and MORB mantle components. Thus, basalts erupting along the Gasitao, Three Magi, and Rodrigues ridges will show a range of $^3\text{He}/^4\text{He}$ ratios values, between the helium isotope composition of lavas from Réunion Island and normal MORB, which may not necessarily be coupled to their trace element and/or radiogenic isotope signatures (Figure 6c).

6. Conclusions

[50] Submarine basaltic glasses recovered from the CIR segment bounded by the Marie Celeste and the Egeria fracture zones record a range in helium isotope compositions, which are decoupled from incompatible trace element ratios. The lowest $^3\text{He}/^4\text{He}$ ratios are observed immediately south of the Marie Celeste FZ, where $(\text{La}/\text{Sm})_N$ ratios are highest. These low $^3\text{He}/^4\text{He}$ values can be explained by closed system radiogenic ^4He ingrowth in a “fossil” Réunion mantle component or, alternatively, fertilized MORB mantle. In contrast, lavas erupting near the Egeria FZ, ~150 km to the south, record normal MORB-like trace element and helium characteristics. Significantly higher $^3\text{He}/^4\text{He}$ ratios (i.e., up to 12.2 R_A) are observed in basaltic glasses between ~19° and 20°S along the CIR axis, as well as along the adjacent Gasitao Ridge, Three Magi Ridges, and Rodrigues Ridge, consistent with lateral flow of hot spot mantle from Réunion

toward the CIR, over a distance of ~1100 km. These high $^3\text{He}/^4\text{He}$ values show that some domains of the expanding hot spot mantle retain their intrinsic high $^3\text{He}/^4\text{He}$ signature. However, since the Réunion mantle component is progressively depleted in incompatible trace elements by melting en route to the CIR, basaltic lavas sampled on the ridge axis at ~19.5°S, i.e., near the present-day intersection of the CIR and the off-axis volcanic structures, show typical N-MORB-like trace element ratios.

[51] **Acknowledgments.** This work was supported by NSF grant OCE-0726573, and the KNOX11RR cruise was funded by UC Ship Funds. We would like to thank Captain T. Desjardins and the crew of the R/V *Reville* for their dedicated support at sea, and the Government of Mauritius is kindly acknowledged for the permission granted to work in the Exclusive Economic Zone. J.M.D.D. acknowledges a *National Geographic Society Research and Exploration* grant (NGS 8330-07). C.H. and J.D. acknowledge CNRS-INSU for funding their participation to the KNOX11RR cruise. We are grateful to Scott Cornelius for major element analyses of olivine separates from the Mascarene Islands. We thank two anonymous reviewers for thorough reviews and André Revil for editorial handling. This is contribution IPGP 3090.

References

- Albarède, F., B. Luais, G. Fitton, M. Semet, E. Kaminski, B. G. J. Upton, P. Bachelery, and J.-L. Cheminée (1997), The geochemical regime of Piton de la Fournaise volcano (Réunion) during the last 530 000 years, *J. Petrol.*, 38(2), 171–201, doi:10.1093/petrology/38.2.171.
- Albers, M., and U. R. Christensen (2001), Channeling of plume flow beneath mid-ocean ridges, *Earth Planet. Sci. Lett.*, 187, 207–220, doi:10.1016/S0012-821X(01)00276-X.
- Allègre, C. J., M. Moreira, and T. Staudacher (1995), $^4\text{He}/^3\text{He}$ dispersion and mantle convection, *Geophys. Res. Lett.*, 22(17), 2325–2328, doi:10.1029/95GL02307.
- Bosch, D., J. Blichert-Toft, F. Moynier, B. K. Nelson, P. Telouk, P.-Y. Gillot, and F. Albarède (2008), Pb, Hf and Nd isotope compositions of the two Réunion volcanoes (Indian Ocean): A tale of two small-scale mantle “blobs”?, *Earth Planet. Sci. Lett.*, 265, 748–765, doi:10.1016/j.epsl.2007.11.018.
- Bottinga, Y., and M. Javoy (1990), MORB degassing: Bubble growth and ascent, *Chem. Geol.*, 81(4), 255–270, doi:10.1016/0009-2541(90)90050-H.
- Burnard, P. G., D. W. Graham, and K. A. Farley (2002), Mechanisms of magmatic gas loss along the Southeast Indian Ridge and the Amsterdam-St. Paul Plateau, *Earth Planet. Sci. Lett.*, 203, 131–148, doi:10.1016/S0012-821X(02)00828-2.
- Carroll, M. R., and D. S. Draper (1994), Noble gases as trace elements in magmatic processes, *Chem. Geol.*, 117(1–4), 37–56, doi:10.1016/0009-2541(94)90120-1.
- Chevallier, L., and P. Bachelery (1981), Evolution structurale du volcan actif du Piton de la Fournaise, Ile de la Réunion, Océan Indien occidental. Structural evolution of the Piton de la Fournaise active volcano, Réunion, western Indian Ocean, *Bull. Volcanol.*, 44(4), 723–741, doi:10.1007/BF02597094.
- Chevallier, L., and N. Vatin-Perignon (1982), Volcano-structural evolution of Piton des Neiges, Reunion Island, Indian Ocean, *Bull. Volcanol.*, 45(4), 285–298, doi:10.1007/BF02597253.
- Day, J. M. D., D. R. Hilton, D. G. Pearson, C. G. Macpherson, B. A. Kjarsgaard, and P. E. Janney (2005), Absence of a high time-integrated $^3\text{He}/(\text{U}+\text{Th})$ source in the mantle beneath continents, *Geology*, 33, 733–736, doi:10.1130/G21625.1.
- Dixon, J. E., E. M. Stolper, and J. R. Holloway (1995), An experimental study of water and carbon dioxide solubilities in mid-ocean ridge basaltic liquids. Part I: Calibration and solubility models, *J. Petrol.*, 36(6), 1607–1631.
- Donnelly, K. E., S. L. Goldstein, C. H. Langmuir, and M. Spiegelman (2004), Origin of enriched ocean ridge basalts and implications for mantle dynamics, *Earth Planet. Sci. Lett.*, 226, 347–366, doi:10.1016/j.epsl.2004.07.019.
- Duncan, R. A., J. Backman, L. Peterson, and The Shipboard Scientific Party (1989), Réunion hot spot activity through Tertiary time: Initial results from the Ocean Drilling Program, Leg 115, *J. Volcanol. Geotherm. Res.*, 36(1–3), 193–198, doi:10.1016/0377-0273(89)90013-9.

- Duncan, R. A., J. Backman, and L. Peterson (1990), The volcanic record of the Réunion hot spot, *Proc. Ocean Drill. Program Sci. Results*, 115, 3–10, doi:10.2973/odp.proc.sr.115.206.1990.
- Dyment, J., Y. Gallet, and the Magfond 2 Scientific Party (1999), The Magfond 2 cruise: A surface and deep tow survey on the past and present Central Indian Ridge, *InterRidge News*, 8, 25–31.
- Dyment, J., C. Hémond, and the Gimnaut Scientific Party (2000), Deep-sea exploration of the Central Indian Ridge at 19°S, *InterRidge News*, 9, 29–32.
- Dyment, J., C. Hémond, H. Guillou, M. Maia, A. Briais, and P. Gente (2001), Central Indian Ridge and Réunion hot spot in Rodrigues area: Another type of ridge-hot spot interaction?, *Eos Trans. AGU*, 82(47), Fall Meet. Suppl., Abstract T31D-05.
- Dyment, J., J. Lin, and E. T. Baker (2007), Ridge-hot spot interactions: What mid-ocean ridges tell us about deep Earth processes, *Oceanography*, 20(1), 102–114.
- Fisk, M. R., R. A. Duncan, A. N. Baxter, J. D. Greenough, R. B. Hargraves, and Y. Tatsumi (1989), Reunion hot spot magma chemistry over the past 65 m.y.: Results from Leg 115 of the Ocean Drilling Program, *Geology*, 17, 934–937, doi:10.1130/0091-7613(1989)017<0934:RHMCO>2.3.CO;2.
- Fretzdorff, S., and K. M. Haase (2002), Geochemistry and petrology of lavas from the submarine flanks of Reunion Island western Indian Ocean: Implications for magma genesis and the mantle source, *Mineral. Petrol.*, 75(3–4), 153–184, doi:10.1007/s007100200022.
- Füri, E., D. R. Hilton, and the KNOX11RR Scientific Party (2008), Sampling and surveying ridge-hot spot interaction on the Central Indian Ridge, 19°S: Cruise KNOX11RR, *InterRidge News*, 17, 28–29.
- Gasparon, M., D. R. Hilton, and R. Varne (1994), Crustal contamination processes traced by helium isotopes: Examples from the Sunda arc, Indonesia, *Earth Planet. Sci. Lett.*, 126, 15–22, doi:10.1016/0012-821X(94)90239-9.
- Gillot, P.-Y., and P. Nativel (1989), Eruptive history of the Piton de la Fournaise volcano, Réunion, Indian Ocean, *J. Volcanol. Geotherm. Res.*, 36(1–3), 53–65, doi:10.1016/0377-0273(89)90005-X.
- Gonnermann, H. M., and S. Mukhopadhyay (2007), Non-equilibrium degassing and a primordial source for helium in ocean-island volcanism, *Nature*, 449, 1037–1040, doi:10.1038/nature06240.
- Graham, D. W. (2002), Noble gas isotope geochemistry of mid-ocean ridge and ocean island basalts: Characterization of mantle source reservoirs, in *Noble Gases in Geochemistry and Cosmochemistry*, Rev. Mineral. Geochem., vol. 47, edited by D. Porcelli et al., pp. 247–317, Mineral. Soc. of Am., Washington, D. C.
- Graham, D. W., W. J. Jenkins, M. D. Kurz, and R. Batiza (1987), Helium isotope disequilibrium and geochronology of glassy submarine basalts, *Nature*, 326, 384–386, doi:10.1038/326384a0.
- Graham, D. W., J. Lupton, F. Albarède, and M. Condomines (1990), Extreme temporal homogeneity of helium isotopes at Piton de la Fournaise, Réunion Island, *Nature*, 347, 545–548, doi:10.1038/347545a0.
- Graham, D. W., K. T. M. Johnson, L. D. Priebe, and J. E. Lupton (1999), Hot spot-ridge interaction along the Southeast Indian Ridge near Amsterdam and St. Paul islands: Helium isotope evidence, *Earth Planet. Sci. Lett.*, 167, 297–310, doi:10.1016/S0012-821X(99)00030-8.
- Hanan, B. B., and J.-G. Schilling (1989), Easter microplate evolution: Pb isotope evidence, *J. Geophys. Res.*, 94(B6), 7432–7448, doi:10.1029/JB094iB06p07432.
- Hanan, B. B., R. H. Kingsley, and J.-G. Schilling (1986), Pb isotope evidence in the South Atlantic for migrating ridge-hot spot interactions, *Nature*, 322, 137–144, doi:10.1038/322137a0.
- Hanyu, T., T. J. Dunai, G. R. Davies, I. Kaneoka, S. Nohda, and K. Uto (2001), Noble gas study of the Reunion hot spot: evidence for distinct less-degassed mantle sources, *Earth Planet. Sci. Lett.*, 193, 83–98, doi:10.1016/S0012-821X(01)00489-7.
- Hart, S. R., J.-G. Schilling, and J. L. Powell (1973), Basalts from Iceland and along Reykjanes Ridge: Sr isotope geochemistry, *Nature*, 246, 104–107.
- Hauri, E. H., J. A. Whitehead, and S. R. Hart (1994), Fluid dynamic and geochemical aspects of entrainment in mantle plumes, *J. Geophys. Res.*, 99(B12), 24,275–24,300, doi:10.1029/94JB01257.
- Hémond, C., A. W. Hofmann, I. Vlastélic, and F. Nauret (2006), Origin of MORB enrichment and relative trace element compatibilities along the mid-Atlantic Ridge between 10° and 24°N, *Geochem. Geophys. Geosyst.*, 7, Q12010, doi:10.1029/2006GC001317.
- Hilton, D. R., K. Hammerschmidt, S. Teufel, and H. Friedrichsen (1993), Helium isotope characteristics of Andean geothermal fluids and lavas, *Earth Planet. Sci. Lett.*, 120, 265–282, doi:10.1016/0012-821X(93)90244-4.
- Hilton, D. R., J. Barling, and G. E. Wheller (1995), Effect of shallow-level contamination on the helium isotope systematics of ocean island lavas, *Nature*, 373, 330–333, doi:10.1038/373330a0.
- Hilton, D. R., G. M. McMurtry, and R. Kreulen (1997), Evidence for extensive degassing of the Hawaiian mantle plume from helium-carbon relationships at Kilauea volcano, *Geophys. Res. Lett.*, 24(23), 3065–3068, doi:10.1029/97GL03046.
- Hilton, D. R., M. F. Thirlwall, R. N. Taylor, B. J. Murton, and A. Nichols (2000), Controls on magmatic degassing along the Reykjanes Ridge with implications for the helium paradox, *Earth Planet. Sci. Lett.*, 183, 43–50, doi:10.1016/S0012-821X(00)00253-3.
- Hopp, J., and M. Trierloff (2005), Refining the noble gas record of the Réunion mantle plume source: Implications on mantle geochemistry, *Earth Planet. Sci. Lett.*, 240, 573–588, doi:10.1016/j.epsl.2005.09.036.
- Ito, G., and J. Lin (1995a), Oceanic spreading center-hot spot interactions: Constraints from along-isochron bathymetric and gravity anomalies, *Geology*, 23, 657–660, doi:10.1130/0091-7613(1995)023<0657:OSCHIC>2.3.CO;2.
- Ito, G., and J. Lin (1995b), Mantle temperature anomalies along the past and paleoaxes of the Galápagos spreading center as inferred from gravity analyses, *J. Geophys. Res.*, 100(B3), 3733–3745, doi:10.1029/94JB02594.
- Ito, G., J. Lin, and C. W. Gable (1997), Interaction of mantle plumes and migrating mid-ocean ridges: Implications for the Galápagos plume-ridge system, *J. Geophys. Res.*, 102(B7), 15,403–15,417, doi:10.1029/97JB01049.
- Ito, G., J. Lin, and D. Graham (2003), Observational and theoretical studies of the dynamics of mantle plume-mid-ocean ridge interaction, *Rev. Geophys.*, 41(4), 1017, doi:10.1029/2002RG000117.
- Jambon, A., H. Weber, and O. Braun (1986), Solubility of He, Ne, Ar, Kr and Xe in a basalt melt in the range 1250–1600°C: Geochemical implications, *Geochim. Cosmochim. Acta*, 50(3), 401–408, doi:10.1016/0016-7037(86)90193-6.
- Jendrzewski, N., T. W. Trull, F. Pineau, and M. Javoy (1997), Carbon solubility in mid-ocean ridge basaltic melt at low pressures (250–1950 bar), *Chem. Geol.*, 138(1–2), 81–92, doi:10.1016/S0009-2541(96)00176-3.
- Kaneoka, I., N. Takaoka, and B. G. J. Upton (1986), Noble gas systematics in basalts and a dunite nodule from Réunion and Grand Comore Islands, Indian Ocean, *Chem. Geol.*, 59(1), 35–42, doi:10.1016/0009-2541(86)90042-2.
- Kincaid, C., G. Ito, and C. Gable (1995), Laboratory investigation of the interaction of off-axis mantle plumes and spreading centres, *Nature*, 376, 758–761, doi:10.1038/376758a0.
- Kincaid, C., J.-G. Schilling, and C. Gable (1996), The dynamics of off-axis plume-ridge interaction in the uppermost mantle, *Earth Planet. Sci. Lett.*, 137, 29–43, doi:10.1016/0012-821X(95)00201-M.
- Kurz, M. D., A. P. Le Roex, and H. J. B. Dick (1998), Isotope geochemistry of the oceanic mantle near the Bouvet triple junction, *Geochim. Cosmochim. Acta*, 62(5), 841–852, doi:10.1016/S0016-7037(97)00383-9.
- Le Roux, P. J., A. P. le Roex, J.-G. Schilling, N. Shimizu, W. W. Perkins, and N. J. G. Pearce (2002), Mantle heterogeneity beneath the southern mid-Atlantic Ridge: Trace-element evidence for contamination of ambient asthenospheric mantle, *Earth Planet. Sci. Lett.*, 203, 479–498, doi:10.1016/S0012-821X(02)00832-4.
- Luais, B. (2004), Temporal changes in Nd isotopic composition of Piton de la Fournaise magmatism (Réunion Island, Indian Ocean), *Geochem. Geophys. Geosyst.*, 5, Q01008, doi:10.1029/2002GC000502.
- Mahoney, J. J., J. H. Natland, W. M. White, R. Poreda, S. H. Bloomer, R. L. Fisher, and A. N. Baxter (1989), Isotopic and geochemical provinces of the western Indian Ocean spreading centers, *J. Geophys. Res.*, 94(B4), 4033–4052, doi:10.1029/JB094iB04p04033.
- Marty, B., and L. Zimmermann (1999), Volatiles (He, C, N, Ar) in mid-ocean ridge basalts: Assessment of shallow-level fractionation and characterization of source composition, *Geochim. Cosmochim. Acta*, 63(21), 3619–3633, doi:10.1016/S0016-7037(99)00169-6.
- McDonough, W. F., and S.-s. Sun (1995), The composition of the Earth, *Chem. Geol.*, 120(3–4), 223–253, doi:10.1016/0009-2541(94)00140-4.
- McDougall, I., and F. H. Chamalaun (1969), Isotopic dating and geomagnetic polarity studies on volcanic rocks from Mauritius, Indian Ocean, *Geol. Soc. Am. Bull.*, 80(8), 1419–1442, doi:10.1130/0016-7606(1969)80[1419:IDAGPS]2.0.CO;2.
- McDougall, I., B. G. J. Upton, and W. J. Wadsworth (1965), A geological reconnaissance of Rodriguez Island Indian Ocean, *Nature*, 206, 26–27, doi:10.1038/206026a0.
- Mellor, S. H. (1998), The geochemistry, petrology and petrogenesis of the Rodrigues Ridge (western Indian Ocean), Ph.D. thesis, 297 pp., Univ. of Greenwich, London.
- Mittelstaedt, E., and G. Ito (2005), Plume-ridge interaction, lithospheric stresses, and the origin of near-ridge volcanic lineaments, *Geochem. Geophys. Geosyst.*, 6, Q06002, doi:10.1029/2004GC000860.
- Montaggioni, L., and P. Nativel (1988), *La Réunion, Ile Maurice - Géologie et Aperçus Biologiques, Plantes et Animaux, Guides Géol. Régionaux*, Masson, Paris.

- Moreira, M., and P. Sarda (2000), Noble gas constraints on degassing processes, *Earth Planet. Sci. Lett.*, *176*, 375–386, doi:10.1016/S0012-821X(00)00010-8.
- Morgan, W. J. (1978), Rodriguez, Darwin, Amsterdam, a second type of hot spot island, *J. Geophys. Res.*, *83*(B11), 5355–5360, doi:10.1029/JB083iB11p05355.
- Morgan, W. J. (1981), Hot spot tracks and the opening of the Atlantic and Indian oceans, in *The Sea*, vol. 7, edited by C. Emiliani, pp. 443–487, Wiley, New York.
- Murton, B. J., A. G. Tindle, J. A. Milton, and D. Sauter (2005), Heterogeneity in southern Central Indian Ridge MORB: Implications for ridge-hot spot interaction, *Geochem. Geophys. Geosyst.*, *6*, Q03E20, doi:10.1029/2004GC000798.
- Nauret, F., W. Abouchami, S. J. G. Galer, A. W. Hofmann, C. Hémond, C. Chauvel, and J. Dymont (2006), Correlated trace element-Pb isotope enrichments in Indian MORB along 18–20°S, Central Indian Ridge, *Earth Planet. Sci. Lett.*, *245*, 137–152, doi:10.1016/j.epsl.2006.03.015.
- Nicolaysen, K. P., F. A. Frey, J. J. Mahoney, K. T. M. Johnson, and D. W. Graham (2007), Influence of the Amsterdam/St. Paul hot spot along the Southeast Indian Ridge between 77° and 88°E: Correlations of Sr, Nd, Pb, and He isotopic variations with ridge segmentation, *Geochem. Geophys. Geosyst.*, *8*, Q09007, doi:10.1029/2006GC001540.
- Nohda, S., I. Kaneoka, T. Hanyu, S. Xu, and K. Uto (2005), Systematic variation of Sr-, Nd- and Pb-isotopes with time in lavas of Mauritius, Réunion hot spot, *J. Petrol.*, *46*(3), 505–522, doi:10.1093/petrology/egh085.
- Okino, K., Y. Ichikawa, and T. Tamaki (2008), Detailed morphology of the Central Indian Ridge between 20deg15S and 15deg30S: Implication for hot spot-ridge interaction, in *Proceedings of the Japan Geoscience Union (JPGU)*, Chiba, Japan, Abstract J164-002.
- Ozima, M., and F. A. Podosek (2002), *Noble Gas Geochemistry*, Cambridge Univ. Press, U. K.
- Parker, R. L., and D. W. Oldenburg (1973), Thermal model of ocean ridges, *Nature Phys. Sci.*, *242*, 137–139.
- Parson, L. M., P. Patriat, R. C. Searle, and A. R. Briais (1993), Segmentation of the Central Indian Ridge between 12°12'S and the Indian Ocean Triple Junction, *Mar. Geophys. Res.*, *15*(4), 265–282, doi:10.1007/BF01982385.
- Paul, D., W. M. White, and J. Blichert-Toft (2005), Geochemistry of Mauritius and the origin of rejuvenescent volcanism on oceanic island volcanoes, *Geochem. Geophys. Geosyst.*, *6*, Q06007, doi:10.1029/2004GC000883.
- Paul, D., V. S. Kamenetsky, A. W. Hofmann, and A. Stracke (2007), Compositional diversity among primitive lavas of Mauritius, Indian Ocean: Implications for mantle sources, *J. Volcanol. Geotherm. Res.*, *164*(1–2), 76–94, doi:10.1016/j.jvolgeores.2007.04.004.
- Pietruszka, A. J., E. H. Hauri, and J. Blichert-Toft (2009), Crustal contamination of mantle-derived magmas within Piton de la Fournaise Volcano, Réunion Island, *J. Petrol.*, *50*(4), 661–684, doi:10.1093/petrology/egp016.
- Porcelli, D., and C. J. Ballentine (2002), Models for the distribution of terrestrial noble gases and the evolution of the atmosphere, in *Noble Gases in Geochemistry and Cosmochemistry*, *Rev. Mineral. Geochem.*, vol. 47, edited by D. Porcelli et al., pp. 412–480, Mineral. Soc. of Am., Washington, D. C.
- Porcelli, D., and G. J. Wasserburg (1995), Mass transfer of helium, neon, argon, and xenon through a steady state upper mantle, *Geochim. Cosmochim. Acta*, *59*(23), 4921–4937, doi:10.1016/0016-7037(95)00336-3.
- Rocholl, A., and K. P. Jochum (1993), Th, U and other trace elements in carbonaceous chondrites: Implications for the terrestrial and solar system Th/U ratios, *Earth Planet. Sci. Lett.*, *117*, 265–278, doi:10.1016/0012-821X(93)90132-S.
- Sarda, P., and D. Graham (1990), Mid-ocean ridge popping rocks: Implications for degassing at ridge crests, *Earth Planet. Sci. Lett.*, *97*, 268–289, doi:10.1016/0012-821X(90)90047-2.
- Scarsi, P. (2000), Fractional extraction of helium by crushing of olivine and clinopyroxene phenocrysts: Effects on the 3He/4He measured ratio, *Geochim. Cosmochim. Acta*, *64*(21), 3751–3762, doi:10.1016/S0016-7037(00)00419-1.
- Schilling, J.-G. (1973), Iceland mantle plume: Geochemical study of Reykjanes Ridge, *Nature*, *242*, 565–571, doi:10.1038/242565a0.
- Schilling, J.-G. (1985), Upper mantle heterogeneities and dynamics, *Nature*, *314*, 62–67, doi:10.1038/314062a0.
- Schilling, J.-G. (1991), Fluxes and excess temperatures of mantle plumes inferred from their interaction with migrating mid-ocean ridges, *Nature*, *352*, 397–403, doi:10.1038/352397a0.
- Schilling, J.-G., R. H. Kingsley, and J. D. Devine (1982), Galápagos hot spot-spreading center system: 1. Spatial petrological and geochemical variations (83°W–101°W), *J. Geophys. Res.*, *87*(B7), 5593–5610, doi:10.1029/JB087iB07p05593.
- Schilling, J.-G., M. Zajac, R. Evans, T. Johnston, W. White, J. D. Devine, and R. Kingsley (1983), Petrologic and geochemical variations along the mid-Atlantic Ridge from 29°N to 73°N, *Am. J. Sci.*, *283*(6), 510–586, doi:10.2475/ajs.283.6.510.
- Schilling, J.-G., G. Thompson, R. Kingsley, and S. Humphris (1985), Hot spot-migrating ridge interaction in the South-Atlantic, *Nature*, *313*, 187–191, doi:10.1038/313187a0.
- Sheth, H., J. Mahoney, and A. Baxter (2003), Geochemistry of lavas from Mauritius, Indian Ocean: Mantle sources and Petrogenesis, *Int. Geol. Rev.*, *45*(9), 780–797, doi:10.2747/0020-6814.45.9.780.
- Sleep, N. H. (1996), Lateral flow of hot plume material ponded at sublithospheric depths, *J. Geophys. Res.*, *101*(B12), 28,065–28,083, doi:10.1029/96JB02463.
- Smith, W. H. F., and D. T. Sandwell (1997), Global sea floor topography from satellite altimetry and ship depth soundings, *Science*, *277*(5334), 1956–1962, doi:10.1126/science.277.5334.1956.
- Staudacher, T., M. D. Kurz, and C. J. Allègre (1986), New noble gas data on glass samples from Loihi Seamount and Huahalai and on dunite samples from Loihi and Réunion Island, *Chem. Geol.*, *56*(3–4), 193–205, doi:10.1016/0009-2541(86)90003-3.
- Staudacher, T., P. Sarda, and C. J. Allègre (1990), Noble gas systematics of Réunion Island, Indian Ocean, *Chem. Geol.*, *89*(1–2), 1–17, doi:10.1016/0009-2541(90)90057-E.
- Sun, S.-s., and W. F. McDonough (1989), Chemical and isotopic systematics of oceanic basalts: Implications for mantle composition and processes, in *Magmatism in the Ocean Basins*, edited by A. D. Saunders and M. J. Norry, *Geol. Soc. Spec. Publ.*, *42*, 313–345, doi:10.1144/GSL.SP.1989.042.01.19.
- Trieloff, M., J. Kunz, and C. J. Allègre (2002), Noble gas systematics of the Réunion mantle plume source and the origin of primordial noble gases in Earth's mantle, *Earth Planet. Sci. Lett.*, *200*, 297–313, doi:10.1016/S0012-821X(02)00639-8.
- van Keken, P. E., E. H. Hauri, and C. J. Ballentine (2002), Mantle mixing: The generation, preservation, and destruction of chemical heterogeneity, *Annu. Rev. Earth Planet. Sci.*, *30*, 493–525, doi:10.1146/annurev.earth.30.091201.141236.
- Vlastélic, I., T. Staudacher, and M. Semet (2005), Rapid change of lava composition from 1998 to 2002 at Piton de la Fournaise (Réunion) inferred from Pb isotopes and trace elements: Evidence for variable crustal contamination, *J. Petrol.*, *46*(1), 79–107, doi:10.1093/petrology/egh062.
- Vlastélic, I., E. Lewin, and T. Staudacher (2006), Th/U and other geochemical evidence for the Réunion plume sampling a less differentiated mantle domain, *Earth Planet. Sci. Lett.*, *248*, 379–393, doi:10.1146/annurev.earth.30.091201.141236.
- White, W. M., M. M. Cheatham, and R. A. Duncan (1990), Isotope geochemistry of Leg 115 basalts and inferences on the history of the Réunion mantle plume, *Proc. Ocean Drill. Prog., Sci. Results*, *115*, 53–61, doi:10.2973/odp.proc.sr.115.131.1990.

J. M. D. Day, Department of Geology, University of Maryland, College Park, MD 20742, USA. (jamesday@geol.umd.edu)

J. Dymont, Laboratoire Géosciences Marines, CNRS UMR 7154, Institut de Physique du Globe de Paris, 1 rue Jussieu, F-75005 Paris, France. (jdy@ipgp.fr)

E. Furi, Centre de Recherche Pétrographiques et Géochimiques, Nancy Université, BP 20, F-54501 Vandoeuvre-lès-Nancy, CEDEX, France. (efuri@crpg.cnrs-nancy.fr)

C. Hémond, UMR “Domaines océaniques,” Institut Universitaire Européen de la Mer, place Nicolas Copernic, F-29280 Plouzané, France. (chhemond@univ-brest.fr)

D. R. Hilton, Fluids and Volatiles Laboratory, Geosciences Research Division, Scripps Institution of Oceanography, University of California, San Diego, La Jolla, CA 92093-0244, USA. (drhilton@ucsd.edu)

B. J. Murton, National Oceanography Centre, University of Southampton, Southampton SO14 3ZH, UK. (bramley.murton@noc.soton.ac.uk)